

Real-Time Model Checking for Closed-Loop Robot Reactive Planning

CHRISTOPHER CHANDLER, University of Glasgow, UK

BERND PORR, University of Glasgow, UK

GIULIA LAFRATTA, University of Glasgow, UK

ALICE MILLER, University of Glasgow, UK

We present a new application of model checking which achieves real-time multi-step planning and obstacle avoidance on a real autonomous robot. We have developed a small, purpose-built model checking algorithm which generates plans *in situ* based on “core” knowledge and attention as found in biological agents. This is achieved in real-time using no pre-computed data on a low-powered device. Our approach is based on chaining temporary control systems which are spawned to counteract disturbances in the local environment that disrupt an autonomous agent from its preferred action (or *resting state*). A novel discretization of 2D LiDAR data sensitive to bounded variations in the local environment is used. Multi-step planning using model checking by forward depth-first search is applied to cul-de-sac and playground scenarios. Both empirical results and informal proofs of two fundamental properties of our approach demonstrate that model checking can be used to create efficient multi-step plans for local obstacle avoidance, improving on the performance of a reactive agent which can only plan one step. Our approach is an instructional case study for the development of safe, reliable and explainable planning in the context of autonomous vehicles.

CCS Concepts: • **Computing methodologies** → **Robotic planning**; • **Software and its engineering** → **Model checking**; • **Computer systems organization** → **Robotic autonomy**; *Real-time system specification*.

Additional Key Words and Phrases: model checking, autonomous vehicles, closed-loop, real-time, planning

1 INTRODUCTION

Biological organisms are embodied agents able to form complex plans and respond flexibly to unexpected events when navigating an environment. This is achieved in real-time without prior experience of encountered situations in a closed-loop fashion based on sensory inputs. Similar to biological organisms, an embodied robotic agent has an egocentric perspective on its surroundings—observations are relative to a local frame of reference and completely dependent on in-built sensors. On sensing an unexpected input (i.e., a “disturbance” representing an obstacle), the agent can respond by performing an action to change its state. This action results in a change to the environment, which is sensed by the agent and the loop repeats until the obstacle is no longer in view [8]. The agent only requires knowledge of the relative position of the obstacle (i.e., disturbance) to perform the action.

This represents a simple reflex response to the environment. However, biological organisms are capable of more sophisticated behaviours, such as the prediction of many consecutive obstacles and the generation of plans to counteract them. As a reflex is only able to react to one obstacle at a time, a single closed-loop controller is insufficient for generating complex multi-step plans. To achieve this, it is necessary for a robotic agent to access and interpret distal sensor information. Indeed, there is evidence that in biological systems an innate “core” understanding of world physics and causality allow organisms to reason about their environment and organise their behaviours in

Authors’ addresses: Christopher Chandler, School of Computing Science, University of Glasgow, Glasgow, Scotland, UK, c.chandler.1@research.gla.ac.uk; Bernd Porr, School of Biomedical Engineering, University of Glasgow, Glasgow, Scotland, UK, bernd.porr@glasgow.ac.uk; Giulia Lafratta, School of Biomedical Engineering, University of Glasgow, Glasgow, Scotland, UK, g.lafratta.1@research.gla.ac.uk; Alice Miller, School of Computing Science, University of Glasgow, Glasgow, Scotland, UK, alice.miller@glasgow.ac.uk.

accordance with predicted outcomes [36, 55]. In other words, organisms have a mental model of the world, allowing them to simulate and evaluate future actions.

One promising computational model of this process characterises “intuitive physical reasoning” in humans as similar to inference over a physics software engine, such as those which power games [4, 35]. According to this hypothesis, we reconstruct a perceptual scene using simplified internal representations of objects and their relevant physical properties. These representations are approximate and oversimplified but rich enough to support mental simulations of objects in the immediate future. Evaluating the outcomes of actions therefore requires the ability to focus attention on objects and their properties. Indeed, this was recently achieved in [34] using a gaming engine on a low-powered robot. This enabled reactive reasoning about the outcomes of closed-loop actions for an unknown scene based on discrete criteria, supporting a broad form of generalisation [12] requiring no prior experience.

Model checking [2] is a widely used technique for automatically verifying reactive systems. It is based on a precise mathematical and unambiguous model of possible system behaviour. To verify that the model meets specified requirements (usually expressed in temporal logic), all possible executions are checked systematically. If an execution failing the specification is found, the execution path which caused the violation is returned. Model checking has been successfully used to ensure the safety and reliability of safety-critical systems such as flight control [59], space-craft controllers [27], and satellite positioning systems [45]. It has also been applied to many aspects of software verification, e.g., to industrial systems [3] and operating systems [57].

In the context of autonomous robots, most research in the field has focused on simulating robotic behaviour in an environment using various levels of abstraction [22, 24, 26, 29, 41, 43, 44, 49]. In some cases model checking has been applied to parts of real autonomous systems [9]. It has been used to check if sensor readings have arrived on time [23], to inspect whether messages in ROS have been corrupted [21, 32], and detect faults in low level robotic control by comparing expected versus actual system readings [5].

In this paper, we explore the use of model checking to generate complex multi-step plans for obstacle avoidance on a real autonomous robot. We do this in a way which reflects the behaviour of biological organisms by generating sequences of closed-loop controllers. The main benefit of our approach is the ability to reason flexibly about the immediate environment based on sensory inputs using a method which is explainable. In comparison, popular black-box AI methods for autonomous navigation (e.g., deep reinforcement learning) make rigid decisions based on generalisations [56] insensitive to the local environment. In safety-critical applications, such as autonomous vehicles (AVs), this undermines the robustness and safety of AI decisions, but also system trustworthiness in general due to the lack of transparency [18].

We focus on two fundamental challenges. As autonomous robots are hybrid systems [52], one challenge is combining discrete control commands and interaction with a continuous environment, which is often partially observable and unstructured [46]. Another challenge is planning in real-time. Standard model checkers are not designed for real-time tasks, hence models are typically verified offline prior to implementation [13, 61] for real-time applications. Online verification of robot behaviour in its environment, however, requires model checkers which can meet hard real-time constraints [1].

This problem was encountered in [48] (extended in [47]), where SPIN [30] and a 3D Unity simulation of an autonomous vehicle were combined to identify paths violating temporal properties for the planning and execution of consecutive overtaking manoeuvres on a traffic-heavy road. The model checker received information from the (simulated) autonomous vehicle, updated its current model, derived a safe path, then communicated the path back to the autonomous vehicle. Although a useful proof-of-concept, the time delay due to both model compilation and communication

between the model checker and game engine was unacceptable (approx. 3 seconds, even though verification of the model itself only took around 20 milliseconds). For this reason, SPIN could not be implemented directly on a robot for real-time planning.

Real-time model checking has only been achieved in a limited number of cases. In [37] model checking was used to generate real-time action plans with formal guarantees for steerable needles [37], however the environment was structured and fully observable. This was also the case for [61] in which industrial robot arms were modelled. In [7] real-time enforcement of safe controls was performed using model checking in an unstructured environment with partial observability. However, only single trajectories were checked, there was no planning involved, and results were validated using simulation. To the best of our knowledge, real-time planning and obstacle avoidance on a real autonomous robot has not yet been achieved using model checking.

We therefore adapt the approach in [48] to a real autonomous agent operating under hard real-time constraints. In the interest of developing a planning method which is also energy efficient, we further constrain our approach by developing on a low-powered robotic platform. Our objective is to demonstrate the effectiveness of two measures which should address the time lag issues identified in [48]: (i) a simplified model checking algorithm whose implementation is shown to satisfy real-time constraints, and (ii) the use of model checking situated *on board* a low-powered autonomous robot. We investigate the reliability of planning using model checking and closed-loop control for safe obstacle avoidance in a case study.

In Section 2, we motivate the limitations of closed-loop control for obstacle avoidance and formulate the reactive planning problem. We give the details of our low-powered platform and provide preliminary concepts and definitions in Section 3. In Section 4, we describe our methodological approach for real-time planning using model checking. We explain the design of our case study and evaluate results in Section 5. In Section 6, we discuss our results and identify limitations. We conclude and comment on future work in Section 7.

Initial findings from our approach were reported in [10]. In this much extended paper we have included a more comprehensive explanation of the methodology and a much wider discussion. We have also extended our experimental results and provided informal proofs of two fundamental properties of our approach which show that it reliably avoids obstacles.

2 MOTIVATING EXAMPLE

Figure 1A shows a robot driving in a straight line until it encounters an obstacle in the environment, represented by disturbance D . This generates an error signal which triggers the agent to output a motor action and change its state. The motor action changes the state of the environment, which is sensed by the robot and the loop repeats until the disturbance D is eliminated.

This simple reflex can be implemented using a closed feedback loop with a strict attentional focus on a single disturbance, as illustrated in Figure 1B. In this paper, we call such a closed-loop controller a “task”. The disturbance D represents an external obstacle which interrupts the “default” state of the robot—driving in a straight line, represented by the task T_0 . In Figure 1A, the task T_R is initiated when the disturbance D comes into view. It has a finite lifetime. Once the disturbance is out of sight, the task T_R is no longer required, so it is terminated and the robot returns to the default task T_0 .

A task feedback loop is a simple mechanism where only information about the disturbance *at the present moment* can be encoded or retained. This means that a task is (i) memoryless and (ii) produces stereotyped behaviour. It has no information on whether it will have to counteract future disturbances as a consequence of its actions, hence a task can only generate a reflex in response to obstacles. This can lead to inefficient agent behaviour.

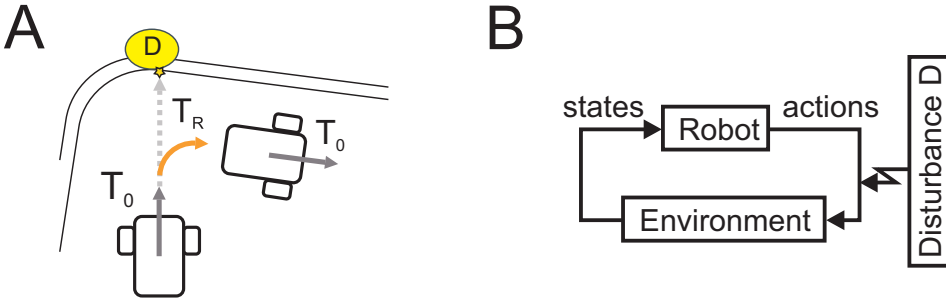


Fig. 1. A: robot encountering an obstacle in its environment, represented as the disturbance D . B: negative feedback loop for the elimination of disturbances.

Figure 2 illustrates one example of a scenario where closed-loop obstacle avoidance on its own may produce undesirable robot behaviour. In both Figures 2A and 2B, the robot starts by executing the default task T_0 . Through distal sensors, the robot receives information that the space ahead contains the disturbance D_1 . Hence it must perform a control action to counteract by rotating either left or right, represented by tasks T_L and T_R , respectively.

From the perspective of the task, either rotation can achieve the control goal of eliminating the disturbance D_1 , so there is no inherent preference. In Figure 2A, the robot initiates task T_L to rotate left until the disturbance D_1 is out of view. The robot can then return to the default task T_0 and safely continue driving straight. However, the robot could have equally chosen to initiate task T_R and rotate right, as shown in Figure 2B. In this case, it would immediately encounter the

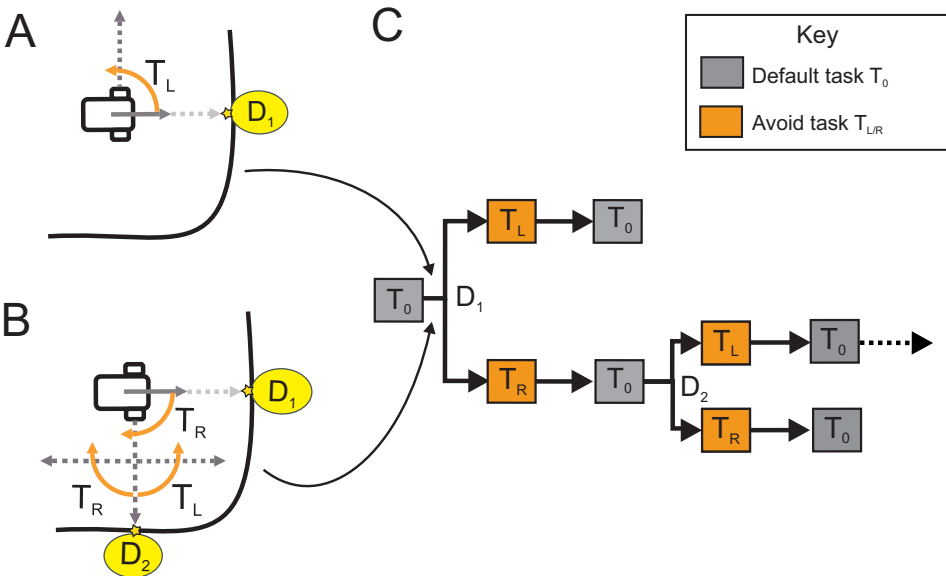


Fig. 2. Uncertainty in corner situation from the perspective of a closed task feedback loop. A and B: valid options for eliminating the disturbance D_1 with varying consequences. C: behaviour tree for reasoning about multiple disturbances to form chains of closed-loop tasks, which requires extending the scope of environment observation.

disturbance D_2 after returning to the default task T_0 . Consequently, the robot must again perform an avoidance manoeuvre. If the robot then initiates task T_R , it would escape the corner and continue in the default task T_0 undisturbed. If the robot initiates task T_L , however, yet another obstacle would be encountered. Hence there is a chance that the robot could get trapped in the corner, which is unwanted behaviour.

It is obvious to an external observer that the behaviour depicted in Figure 2A is more efficient and therefore desirable. As a closed feedback loop can only encode and retain information about an immediate disturbance, however, choosing the most efficient option for obstacle avoidance is impossible. This requires extending the scope of reasoning beyond the present moment.

In this paper, we use model checking to explore *future* system states resulting from the execution of task sequences which satisfy an invariance constraint for obstacle avoidance. Our aim is to reason about possible chains of closed-loop tasks, as illustrated by the behaviour tree shown in Figure 2C.

3 PRELIMINARIES

In this section, basic notions are introduced to motivate the development of our method. We give details on our robotic research platform and sensing capabilities in Section 3.1, define the high-level architecture of our robotic agent in Section 3.2, and provide relevant formal definitions in Section 3.3.

3.1 Robotic Platform

We developed our method on a low-powered robot shown in Figure 3. Our robot was adapted from a widely available mobile robot development platform, AlphaBot by Waveshare¹. For sensing the environment, we equipped the robot with a low cost 360 degree 2D laser scanner, RPLiDAR A1M8 by Slamtec², and for actuation we used two continuous rotation servos by Parallax³. The hardware programming interface for the robot was a Raspberry Pi 3 Model B⁴ included with the AlphaBot development kit running a Quad Core 1.2GHz Broadcom 64bit CPU with 1GB RAM and wireless LAN.

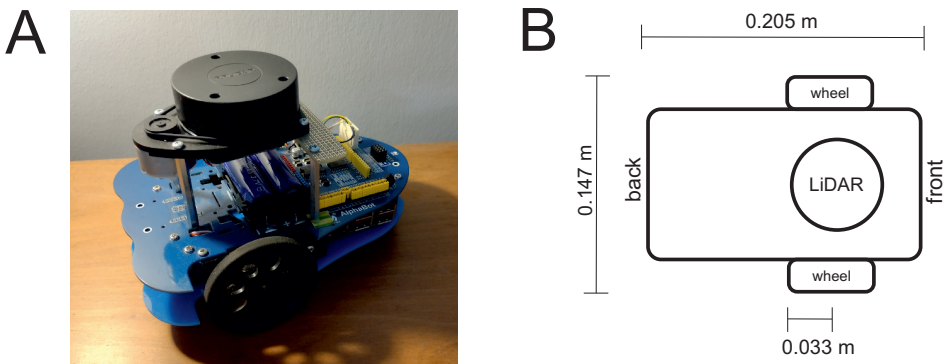


Fig. 3. A: our robotic platform. B: schematic showing robot dimensions.

¹<https://www.waveshare.com/alphabot-robot.htm>

²<https://www.slamtec.com/en/LiDAR/A1/>

³<https://www.parallax.com/product/parallax-continuous-rotation-servo/>

⁴<https://www.raspberrypi.com/products/raspberry-pi-3-model-b/>

The LiDAR generates a 2D point cloud at a rate of ≈ 5 Hz. We use a 2D vector space to model the point cloud with the origin representing a point at the centre of the LiDAR. The robot is oriented towards positive x by convention which corresponds to the heading 0 radians. Rotating 90 degrees left is equivalent to the heading $\frac{1}{2}\pi$ radians, and rotating 90 degrees right is equivalent to the heading $-\frac{1}{2}\pi$ radians. The maximum heading is π in the left direction and $-\pi$ in the right, representing a 180 degrees rotation relative to the local frame.

3.2 Agent Architecture

Figure 4 shows the agent architecture. Our focus is on planning sequences of discrete closed-loop control tasks using in-built sensors to promote reactivity to imminent collisions. During execution, the robot reasons about current task outcomes. When a disturbance is encountered, model checking is used to reason about the outcomes of future tasks and possible task sequences. This separation of concerns is reflected in the architecture shown in Figure 4. Our agent is implemented in C++ using an event-driven paradigm⁵.

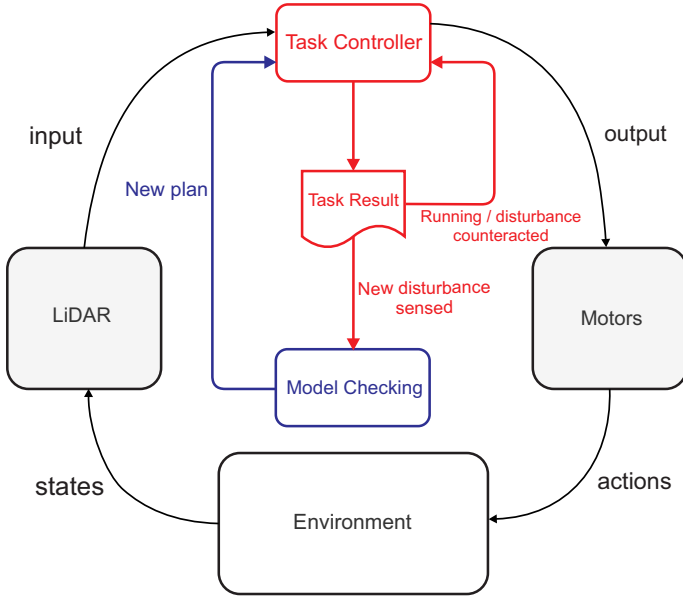


Fig. 4. Agent architecture. Red indicates reasoning based on current task outcomes. Blue indicates planning using model checking based on future task outcomes.

3.3 Model Checking as Planning

We use Linear Temporal Logic (LTL) for plan specification due to its power for planning discrete sequential tasks. LTL formulae over the set AP of atomic propositions are formed according to the grammar [2]:

$$\varphi ::= \text{true} \mid a \mid \varphi_1 \wedge \varphi_2 \mid \neg\varphi \mid \bigcirc\varphi \mid \varphi_1 \cup \varphi_2 \quad (1)$$

where a is an atomic proposition and an indexed φ_i denotes some arbitrary but distinct formula in LTL. From this basic grammar, other operators can be derived, such as \square (“always”) and \diamond

⁵<https://zenodo.org/records/15382644>

(“eventually”), however the derivation is omitted here for brevity (see [2] for a detailed discussion). Note that any LTL property is assumed to hold for all paths.

Our approach utilises a single regular property φ defined in relation to a discrete model of possible system behaviour. In model checking, we are normally interested in verifying that a property holds for all possible runs of a system to provide formal guarantees that the system model satisfies the specification. If the property is violated during a run, a counterexample is returned giving the path of states that lead to the error.

In this paper, we are interested in counterexamples as *solution paths*. For our property φ , there exists a nondeterministic finite automaton (NFA) $\mathcal{A}_{\neg\varphi} = (Q, \Sigma, \delta, Q_0, F)$ where Q is a finite set of states, $\Sigma = 2^{AP}$ is a finite alphabet defined as the the set of all subsets of AP , $\delta : Q \times \Sigma \rightarrow 2^Q$ is a transition relation, $Q_0 \subseteq Q$ is a set of initial states, and $F \subseteq Q$ is a set of accepting states [2]. The NFA can accept all *finite* paths that satisfy $\neg\varphi$.

We use a finite transition system to model the behaviour of the robot. A finite transition system TS is a tuple $(S, Act, \rightarrow, I, AP, L)$ where S is a finite set of states, Act is a finite set of actions, $\rightarrow \subseteq S \times Act \times S$ is a transition relation, $I \subseteq S$ is a set of initial states, AP is a finite set of atomic propositions, and L is a labelling function that determines which atomic propositions are true at each state.

Checking whether φ holds for all finite runs of a transition system TS is equivalent to checking that the automaton formed as the product of the set of finite paths and NFA $\mathcal{A}_{\neg\varphi}$ has no accepting paths. We do not give details here, but provide examples in Section 4.4.2. Note that to check for infinite path violations of a property we would use a Büchi automaton [58] rather than an NFA, but that is not required in this paper.

4 METHODOLOGY

In this section, we explain the details of our approach for real-time planning using model checking. We define the action space and set of closed-loop tasks for our approach in Section 4.1. In Section 4.2, we describe how we abstract closed-loop behaviours using spatial relationships. We describe the transition system used in our approach in Section 4.3. In Section 4.4, we explain how we use an LTL property to specify and generate plans at runtime.

4.1 Action Space

We define the action space for our approach as the set of tasks:

$$Act = \{T_0, T_S, T_L, T_R\} \quad (2)$$

introduced in Section 2. Note that in the default task T_0 the robot has the expectation that it can continue driving in a straight line for a (potentially) infinite period of time—until a disturbance D is encountered. Consequently, the robot has the expectation that the path ahead is finite, so the default task becomes the finite straight task T_S . This also holds for intermediary straight tasks in a plan because the robot has reasoned that it can only drive straight for a finite period. Hence our approach utilises two straight tasks.

4.2 Abstract Closed-Loop Sequences

As explained in Section 2, a task feedback loop has an attentional focus on an immediate disturbance, hence it cannot predict whether it will be necessary for a robot to counteract a future disturbance as a consequence of its execution. To achieve this, a robotic agent requires the ability to access and interpret distal sensor information. In this paper, we abstract away the timed aspects of closed-loop tasks and represent their continuous evolution with spatial constructions, defined in relation to

2D LiDAR data. This makes it possible to reason about the consequences of task execution and strategies to counteract future disturbances. We also require that the robot returns to the default task T_0 as soon as possible without executing consecutive avoid tasks, a bias which we operationalise by ensuring that the robot prefers selecting the shortest safe sequence meeting this requirement.

In the remainder of this section, we explain how we reason about the safety of future task execution for two, three, and four step sequences. We do this in order of sequence length. First we reason about two step sequences, as they return to the default task T_0 after executing a single avoid task $T_{L/R}$. If this is not possible, we then move on to reason about three step sequences. This is a safety feature for situations where there is no lateral room for manoeuvre, however it involves executing two consecutive avoid tasks. If a three step plan is deemed unnecessary, we then move on reason about the safety of four step sequences, which do not involve consecutive avoid tasks.

4.2.1 Two Step Sequences. The shortest possible sequence of tasks is two steps. This represents a situation where the robot encounters a disturbance, executes a single avoid task $T_{L/R}$ then returns to the default task T_0 because no future disturbance has been predicted as a consequence of driving straight in the lateral dimension, as illustrated by the motivational example in Figure 2A for a left turn.

Note that to determine whether a straight task is a success or failure, we define partitions in front of the robot. As shown in Figure 5A, there are two partitions, P_{look} and P_{shield} . If the robot is in the default task T_0 , it is a success during execution. However, if a disturbance is witnessed in P_{look} , then the task T_0 is a failure. This triggers the generation of a new plan. If the robot is in the straight task T_S , the task is again a success during execution. The task is a failure if a disturbance is witnessed in partition P_{shield} which triggers the next task in a plan, or stops the robot if the plan is empty.

Based on the example in Figure 2A, we first explain reasoning about safety for two step sequences, in this case for a left turn where no second disturbance prevents the robot from returning to the default task T_0 . A detailed example of this is shown in Figure 5A where the robot encounters disturbance D^+ after successfully driving straight in the default task T_0 . The robot then witnesses a disturbance in the partition P_{look} (not shown) which indicates that the task is a failure and triggers the generation of a new plan, the sequence $T_L \rightarrow T_0$. As the robot has information that there is a disturbance straight ahead, it now has the expectation that the future path is finite, so continues driving straight in task T_S until the disturbance D^+ is witnessed in partition P_{shield} . This indicates that task T_S is a failure which triggers the first task in the plan. In our example, this is the avoid task T_L .

To ensure an avoid task (i.e., rotation) is safe in our approach, we construct an egocentric safe zone around the robot (dotted circle in Figure 5A) defined by the radius d_{safe} . No object is allowed inside the safe zone. During execution, we consider an avoid task a failure until the absolute difference between the current and initial angles of the disturbance is greater than $\frac{1}{2}\pi$. Consequently, the task is a success which triggers the next task in the plan.

For reasoning about the safety of future straight tasks in the lateral dimension we construct lateral partitions of the state space. We iterate over the set of observations O and subtract a longitudinal offset $\Delta^+ = D_x^+ - d_{safe}$ from the x -coordinate to simulate witnessing D^+ as a proximal disturbance in the future. (Note that in this paper we use the subscript D_x^+ to denote the x -coordinate of a disturbance and the subscript D_y^+ to denote the y -coordinate.) We then construct a lateral partition for the left direction:

$$P_L = \{o \in O \mid |o_x| \leq d_{safe} \wedge 0 < \min(o_y) \leq d_{max}\} \quad (3)$$

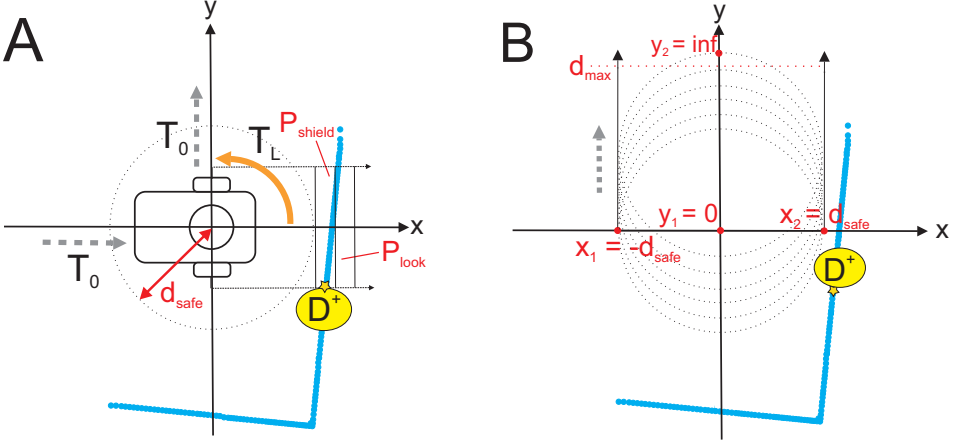


Fig. 5. A: closed-loop execution of the two step sequence $T_L \rightarrow T_0$. B: spatial abstraction of the closed-loop sequence in A which in this case witnesses no disturbances.

where d_{safe} is a bound on the longitudinal dimension to respect the combined safe zone and outer shield $r + d_{shield}$, 0 is a lower bound on the lateral dimension, and d_{max} is an upper bound indicating a maximum lateral look ahead distance for witnessing distal disturbances. As shown in Figure 5B, the partition P_L is empty, so returning to the default task T_0 is possible.

However, there could have been a second disturbance preventing the robot from returning to the default task, as illustrated by the example in Figure 2B for a right turn. Figure 6A shows a detailed example of the robot executing a right turn in response to D^+ , i.e., the sequence of tasks $T_R \rightarrow T_0$. In this case, the robot encounters the disturbance D^R in the right direction as a consequence of executing the avoid task T_R which is again safe due to construction of the safe zone. It is therefore only necessary to reason about the safety of driving straight in the lateral dimension. As the geometry of task execution is symmetrical to the previous sequence, we can iterate over the set of observations and construct the negative reflection of Equation 3:

$$P_R = \{o \in O \mid |o_x| \leq d_{safe} \wedge -d_{max} \leq \max(o_y) < 0\} \quad (4)$$

where d_{safe} is a bound on the longitudinal dimension respecting the combined safe zone and outer shield, 0 is an upper bound on the lateral dimension, and $-d_{max}$ is a lower bound indicating a maximum look ahead distance for witnessing distal disturbances in the right direction. As shown in Figure 6B, the partition P_R is not empty, so returning to the task T_0 is not possible.

Table 1 summarises outcomes for two step sequences in terms of the left and right lateral partitions defined in Equations 3 and 4, respectively.

Table 1. Possible outcomes for two step sequences.

Sequence	Success	Failure
$T_L \rightarrow T_0$	$P_L = \emptyset$	$P_L \neq \emptyset$
$T_R \rightarrow T_0$	$P_R = \emptyset$	$P_R \neq \emptyset$

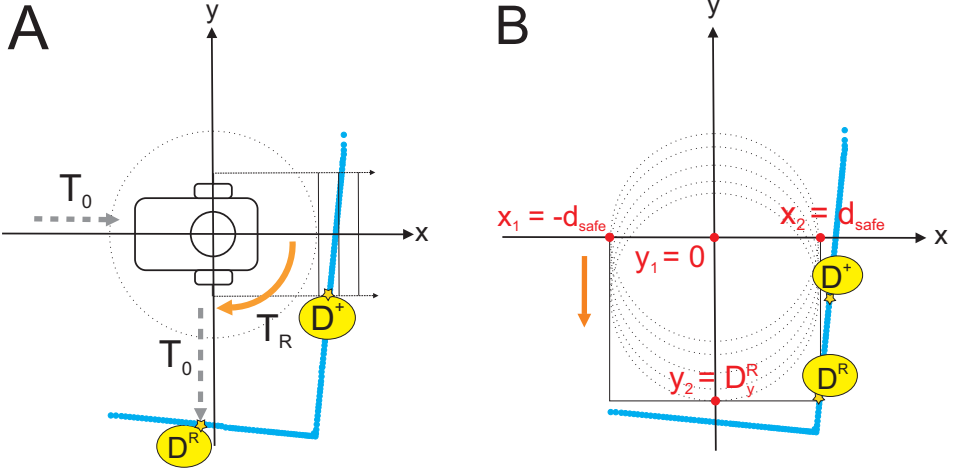


Fig. 6. A: closed-loop execution of the two step sequence $T_R \rightarrow T_0$. B: spatial abstraction of the closed-loop sequence in A which in this case witnesses disturbance D_R .

Success or failure for either sequence (i.e., whether the robot is able to return to the default task T_0) can therefore be expressed as satisfaction of an existential condition in first order logic over the relevant partition:

$$P_L \models \exists D (|D_x| \leq d_{safe} \wedge 0 < D_y \leq d_{max}) \quad (5)$$

$$P_R \models \exists D (|D_x| \leq d_{safe} \wedge -d_{max} \leq D_y < 0) \quad (6)$$

The procedure for constructing lateral partitions is provided in Algorithm 1.

4.2.2 Three Step Sequences. In the event that a two step sequence it not possible, we check whether the robot is in a situation where it is “boxed in” (i.e., it does not have sufficient space in either lateral direction to drive straight for a minimum distance d_{min} without encountering a second disturbance). In this case, the robot can execute either the sequence $T_L \rightarrow T_L \rightarrow T_0$ or sequence $T_R \rightarrow T_R \rightarrow T_0$ to turn around and go back the way it came, otherwise a three step plan is unnecessary and we move on to consider a four step plan (see Section 4.2.3). Options for three step plans are restricted by our model (details provided in Section 4.3). As we restrict our attention to static environments, we can assume that returning to the default task T_0 after turning around is safe.

We use the lateral dimension to reason about whether the robot can move distance d_{min} in either direction. If the robot is boxed in, Equations 5 and 6 are both satisfied, so the union $P_L \cup P_R$ models the disjunction. Hence Equations 5 and 6 together form independently necessary but jointly sufficient conditions for reasoning about whether the robot has enough room to manoeuvre. As P_L and P_R are disjoint, we then construct a third partition:

$$P_{min} = \{D \in P_L \cup P_R \mid -d_{min} \leq D_y \leq d_{min}\} \quad (7)$$

which is a proper subset of $P_L \cup P_R$. Hence the intersection $P_{min} \cap (P_L \cup P_R)$ overlaps both partitions by definition and includes all disturbances relevant for deciding if a three step plan is necessary. We can then define the set:

$$E = \{\langle D^L, D^R \rangle \mid D^L \in P_{min} \cap P_L \wedge D^R \in P_{min} \cap P_R\} \quad (8)$$

Algorithm 1: Construct Lateral Partition

Input : Simulated observations O , parameter d_{safe} , parameter d_{max} , and boolean flag $left$ indicating whether the partition should be in the left or right lateral direction.

Output: The left or right lateral partition P .

```

1 Procedure ConstructPY( $O, d_{safe}, d_{max}, left$ )
2    $P \leftarrow \emptyset$ 
3   for  $o \in O$  do
4     if  $|o_x| \leq d_{safe}$  then
5       if  $left \wedge 0 < o_y \leq d_{max}$  then
6         /* positive partition */
7         add  $o$  to  $P$ 
8       else if  $\neg left \wedge -d_{max} \leq o_y < 0$  then
9         /* negative partition */
10        add  $o$  to  $P$ 
11    $P \leftarrow \text{FilterNearest}(P, d_{max})$ 
12   return  $P$ 

11 Procedure FilterNearest( $P, d_{max}$ )
12    $P' \leftarrow \emptyset$ 
13    $D \leftarrow \emptyset$ 
14    $min \leftarrow d_{max}$ 
15   for  $o \in P$  do
16     if  $|o_y| < min$  then
17        $min \leftarrow |o_y|$ 
18        $D \leftarrow o$ 
19   add  $D$  to  $P'$ 
20   return  $P'$ 

```

where D^L is a disturbance in partition P_L and D^R is a disturbance in partition P_R . We then use the set to reason whether the robot can move in at least lateral direction. If the set E is non-empty, there is a disturbance at most distance d_{min} in both lateral directions, hence we can reason that the robot is boxed in and a sequence of length three is generated to turn around and evade. If the set E is empty, then a three step plan is unnecessary.

4.2.3 Four Step Sequences. The final sequence length is four steps, which is required in a situation where there is a disturbance in some lateral direction but the distance is greater than d_{min} . Hence the robot can drive safely in some lateral direction for a while but then must counteract a second disturbance. For example, the robot can execute the sequence $T_L \rightarrow T_S \rightarrow T_L \rightarrow T_0$ which includes an intermediate straight task. As we reason about the safety of sequences in order of increasing length, we have already reasoned that the first subsequence $T_L \rightarrow T_S$ is safe. Hence we only need to consider whether $T_L \rightarrow T_0$ would be safe to execute after the initial two steps.

We first simulate the lateral displacement of the robot. We calculate the lateral offset $\Delta^L = D_y^L - d_{safe}$ and subtract this from the y -coordinates of observations to simulate the expected state change from executing the subsequence $T_L \rightarrow T_0$ while respecting the safe zone. Note that as we

are reasoning about spatial abstractions, lateral translation of the state space is sufficient, so it is unnecessary to simulate rotations. It is now possible to reason about the final subsequence $T_L \rightarrow T_0$ in the longitudinal dimension by constructing longitudinal partitions. The procedure is the same whether we have simulated driving straight in either the left or right direction.

We iterate over the set of observations and construct the positive partition

$$P^+ = \{o \in O \mid d_{safe} < o_x \leq d_{safe} + \beta d_{safe} \wedge |o_y| \leq \frac{1}{2}(L + tol)\} \quad (9)$$

where d_{safe} is a lower bound on the longitudinal dimension which excludes the lateral partition, $d_{safe} + \beta d_{safe}$ is an upper bound with a tunable coefficient β , and $\frac{1}{2}(L + tol)$ is a bound on the lateral dimension to respect the width of the robot plus some tolerance. In our example, we assume that a disturbance is witnessed in partition P^+ , hence we can conclude that it is not possible to return to the default task T_0 by driving in the positive direction.

We then iterate over the set O and construct the negative partition:

$$P^- = \{o \in O \mid -(d_{safe} + \beta d_{safe}) \leq o_x < -d_{safe} \wedge |o_y| \leq \frac{1}{2}(L + tol)\} \quad (10)$$

where $-(d_{safe} + \beta d_{safe})$ is a lower bound on the longitudinal dimension with the tunable coefficient β , $-d_{safe}$ is an upper bound which again excludes the lateral partition, and $\frac{1}{2}(L + tol)$ is again a bound on the lateral dimension to respect the width of the robot. In our example, we assume that the negative longitudinal partition P^- is empty, so we can conclude that driving straight in the negative longitudinal direction has a (potentially) infinite lifetime. Hence it is possible for the robot to return to the default task T_0 .

Table 2 summarises the possible future outcomes for final subsequences in a four step sequence in terms of the positive and negative longitudinal partitions defined in Equations 9 and 10, respectively. While our example has focused on the left lateral direction, in practice both directions are assessed for completeness. The same procedure applies to the right direction by a symmetrical argument. Note that we refer to longitudinal partitions in the left lateral direction as P_L^\pm and P_R^\pm in the right lateral direction, however this distinction is omitted where directionality is irrelevant.

Table 2. Possible outcomes for final subsequence of four step sequences.

Lateral Offset	Subsequence	Success	Failure
$\Delta^L = D_y^L - d_{safe}$	$T_R \rightarrow T_0$	$P_L^+ = \emptyset$	$P_L^+ \neq \emptyset$
	$T_L \rightarrow T_0$	$P_L^- = \emptyset$	$P_L^- \neq \emptyset$
$\Delta^R = D_y^R + d_{safe}$	$T_R \rightarrow T_0$	$P_R^- = \emptyset$	$P_R^- \neq \emptyset$
	$T_L \rightarrow T_0$	$P_R^+ = \emptyset$	$P_R^+ \neq \emptyset$

Success and failure for either subsequence can again be expressed as satisfaction of an existential condition in first order logic over the relevant partition:

$$P^+ \models \exists D(d_{safe} < D_x \leq d_{safe} + \beta d_{safe} \wedge |D_y| \leq \frac{1}{2}(L + tol)) \quad (11)$$

$$P^- \models \exists D(-(d_{safe} + \beta d_{safe}) \leq D_x < -d_{safe} \wedge |D_y| \leq \frac{1}{2}(L + tol)) \quad (12)$$

The procedure for constructing the partitions is provided in Algorithm 2.

Algorithm 2: Construct Longitudinal Partition

Input : Simulated observations O , lateral offset $\Delta^{L/R}$, parameter d_{safe} , width of the robot plus some tolerance $L + tol$, boolean flag *positive* indicating sign of partition.

Output : The positive or negative longitudinal partition P .

```

1 Procedure ConstructPX( $O, \Delta^{L/R}, d_{safe}, L + tol, positive$ )
2    $P \leftarrow \emptyset$ 
3   for  $o \in O$  do
4      $o_y \leftarrow o_y - \Delta_y$  // simulate lateral displacement
5     if  $|o_y| \leq \frac{1}{2}(L + tol)$  then
6       if  $positive \wedge d_{safe} < o_x \leq d_{safe} + \beta d_{safe}$  then
7         /* positive partition */
8         add  $o$  to  $P$ 
9       else if  $\neg positive \wedge -(d_{safe} + \beta d_{safe}) \leq o_x < -d_{safe}$  then
10        /* negative partition */
11        add  $o$  to  $P$ 
12   return  $P$ 

```

4.3 Disturbance-Focused Transition System

The abstraction approach discussed in Section 4.2 motivates the construction of an egocentric transition system representing possible task sequences. This can be viewed as a mental model encoding “core” knowledge [55] about the temporal evolution of closed-loop tasks and possible disturbances which may be encountered as a consequence of their execution. Hence we maintain a strict attentional focus on disturbances in our model, where a disturbance (i.e., obstacle) is conceived as the cause of a task.

Our model comprises 15 states. Figures 7A and 7B show the positions of states s_0, s_1 and s_2 relative to the robot. To ensure the safe zone is respected, we offset all states in the transition system distance d_{safe} from either the origin or a lateral disturbance. Hence we have one initial state in our model $s_0 = [d_{safe}, 0, 0]$ which is offset distance d_{safe} from the origin of the vector space. As our approach is egocentric, the heading 0 radians indicates the direction the robot always faces, hence all paths in our model start from the initial state s_0 . The states $s_1 = [0, d_{safe}, \frac{1}{2}\pi]$ and $s_2 = [0, -d_{safe}, -\frac{1}{2}\pi]$ represent transitions T_L and T_R , respectively, from s_0 and are fixed.

States s_3 and s_4 represent the outcome of driving straight in the lateral direction from states s_1 and s_2 , respectively, but their valuation varies depending on the location of lateral disturbances. As shown in Figure 7A, if there are none, then as the lateral partitions are empty, we assume that $s_3 = [0, \infty, \frac{1}{2}\pi]$ and $s_4 = [0, -\infty, -\frac{1}{2}\pi]$, meaning that it is possible for the robot to drive in either direction for a (potentially) infinite period of time, so the relevant transition to s_3 or s_4 is the default task T_0 . Hence both Equations 5 and 6 are not satisfied, meaning that a two step sequence in either direction is possible. However, if there are lateral disturbances, both states would have a finite valuation such that $s_3 = [0, D_y^L, \frac{1}{2}\pi]$ and $s_4 = [0, D_y^R, -\frac{1}{2}\pi]$, as shown in Figure 7B. As the lateral partitions are not empty, the robot can only drive for a finite amount of time in either direction, so the relevant transition is the straight task T_5 . In this case, both Equations 5 and 6 are satisfied, meaning that a two step sequence in either direction is *not* possible.

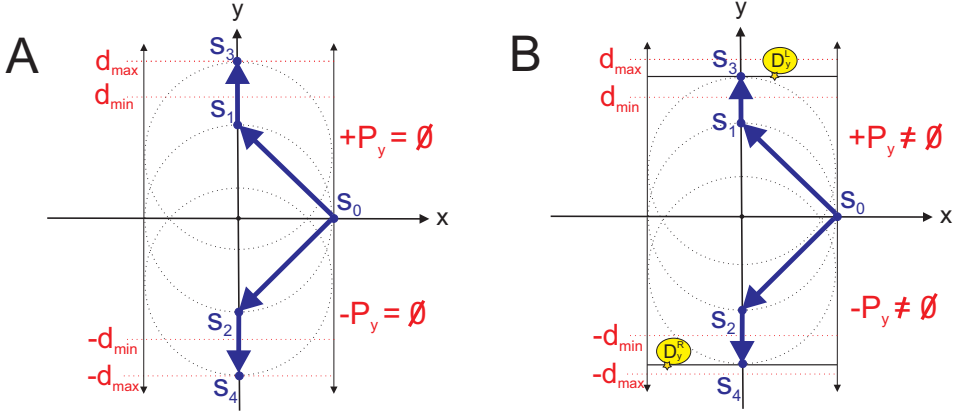


Fig. 7. States for two step sequences. A: lateral partitions with no distal disturbances detected. B: lateral partitions with distal disturbances detected.

Figure 8A shows two additional states in our transition system required for considering the possibility of a three step plan. State $s_{13} = [-d_{safe}, 0, \pi]$ is fixed in our model and represents the execution of a second avoid task $T_{L/R}$ from either state s_1 or s_2 . The state $s_{14} = [-d_{safe} + \beta d_{safe}, 0, \pi]$ represents the final transition T_0 which is assumed safe in our approach, as the robot should be able to go back the way it came in static environments without encountering a disturbance. Starting from the initial state s_0 , this would result in either the sequence $T_L \rightarrow T_L \rightarrow T_0$ or $T_R \rightarrow T_R \rightarrow T_0$, which is chosen non-deterministically, as either sequence would result in the robot going back the way it came. If Equation 8 is satisfied, then a three step sequence is possible, otherwise we move on to consider a four step sequence.

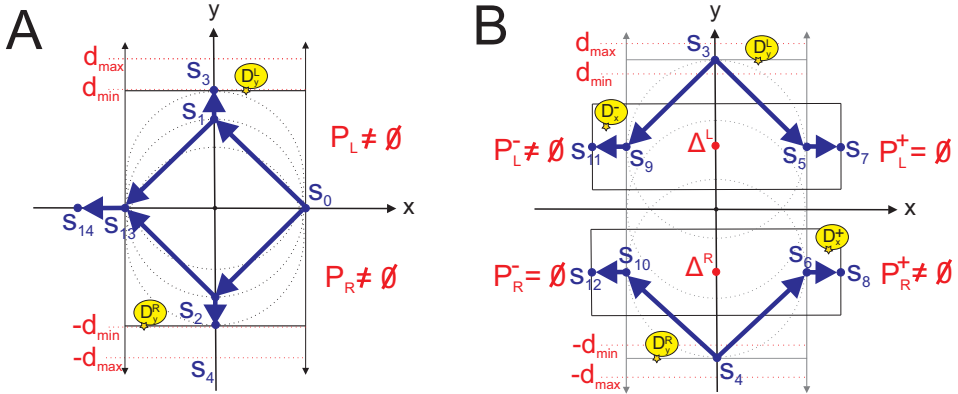


Fig. 8. States for three and four step sequences. A: states for three step sequence. B: states for the final subsequence of a four step sequence.

Figure 8B shows the positions of states for assessing longitudinal movements, representing the final subsequence in four step sequences. States $s_9 = [-d_{safe}, \Delta^L, \pi]$ and $s_5 = [d_{safe}, \Delta^L, 0]$ represent the transitions T_L and T_R , respectively, from state s_3 in the left lateral direction. The longitudinal dimension is fixed but the lateral dimension varies relative to the location of the

left lateral disturbance D^L (see Table 2 for the definition of Δ^L). If the longitudinal partitions are empty then $s_{11} = [-\infty, \Delta^L, \pi]$ and $s_7 = [\infty, \Delta^L, 0]$. Equations 11 and 12 are therefore satisfied, so we can assume the robot can drive in either longitudinal direction for a (potentially) infinite period of time. If the longitudinal partitions are not empty, then $s_{11} = [-(d_{safe} + \beta d_{safe}), \Delta^L, \pi]$ and $s_7 = [d_{safe} + \beta d_{safe}, \Delta^L, 0]$. Hence Equations 11 and 12 are not satisfied, so returning to the default task T_0 is not possible. Note that the same holds for the set of states $\{s_4, s_6, s_8, s_{10}, s_{12}\}$ in the right direction by a symmetrical argument. The resulting transition system is depicted in Figure 9 and defined in Definition 1.

DEFINITION 1. [*Disturbance-Focused Transition System*] A disturbance-focused transition system *DTS* is a tuple $(S, Act, \rightarrow, I, AP, L)$ where

- $S = \{s_0, s_1, \dots, s_{14}\}$ is a set of states where the orientation of the robot is fixed, the longitudinal and lateral dimensions are fixed for states $\{s_0, s_1, s_2, s_{13}, s_{14}\}$, and for the remaining states the longitudinal or lateral dimensions vary in relation to disturbances;
- $Act = \{T_0, T_S, T_L, T_R\}$ is the set of tasks defined in Section 4.1;
- $\rightarrow \subseteq S \times Act \times S$ is a transition relation where $s \rightarrow s'$ is admissible if and only if a task can evolve the model from state s to s' ;
- $I = \{s_0 = [d_{safe}, 0, 0]\}$ is the initial state;
- AP is a set of atomic propositions;
- $L : S \rightarrow 2^{AP}$ is a labelling function which determines which elements of AP are true at each state s .

States in our model receive a valuation (labelling) at runtime using the abstraction approach described in Section 4.2, based on the location of disturbances. We provide examples of label assignment in the next section.

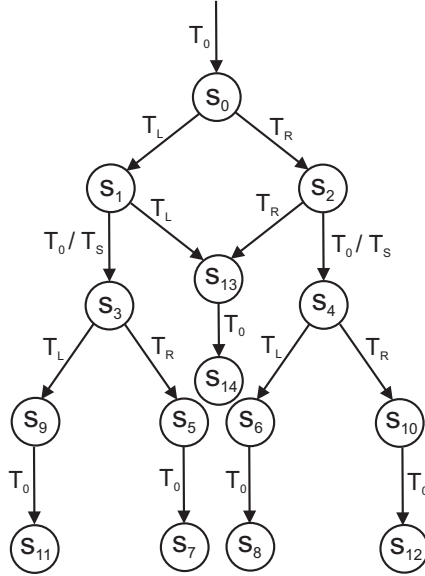


Fig. 9. Disturbance-focused transition system.

4.4 Planning Using Model Checking

We use the *disturbance-focused* transition system described in the previous section to generate plans for negotiating multiple disturbances using distal sensor information. To do this we define an LTL property, construct a non-deterministic finite automaton (NFA) and form the product transition system and NFA for a valuation of state properties based on sensor data.

We implement the underlying directed graph for the finite transition system shown in Figure 9 and compute the product at runtime when a new planning sequence is initiated. Hence planning using model checking can be reduced to a reachability analysis on the product, which amounts to simply deciding which states in the graph are terminal. As indicated in Section 4.2, we reason about the transition system in order of increasing sequence length to ensure reasoning about safety accumulates for each plan length.

4.4.1 LTL Plan Specification. To specify plans for our approach, we define a regular property in LTL which is stated in terms of a set of two state properties, *horizon* and *safe*. Before introducing the LTL property, we define these state properties.

DEFINITION 2. *Property horizon is true at state s if and only if the valuation of either the longitudinal or lateral dimension is infinite.*

In Definition 2 an infinite dimension in the valuation of a state means that the robot can drive in a straight line for a (potentially) infinite period of time, so it can return to the default task T_0 . If the future path of the robot seems infinite, then there is no known disturbance ahead, so by definition it is deemed safe. Our definition of the state property *safe* is less straightforward.

DEFINITION 3. *Property safe is true at state s if one of the following conditions hold: (i) the absolute value of one finite dimension at s is d_{safe} ; (ii) s has a finite lateral dimension such that the absolute distance of a lateral disturbance is greater than parameter d_{min} and there is no longitudinal dimension; or (iii) proposition horizon is true at s.*

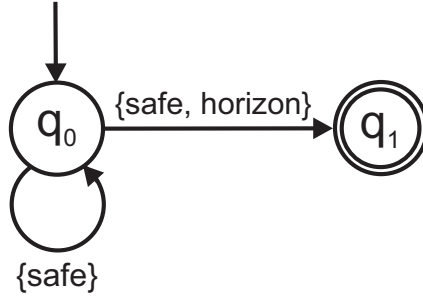
In Definition 3 condition (i) ensures rotations are safe due to construction of the safe zone and outer shield for witnessing proximal disturbances. The value of one dimension is equal to d_{safe} for relevant states around the origin and this uniquely identifies them. Condition (ii) ensures that the robot has space to move in the lateral direction while respecting the safe zone. The final condition (iii) guarantees that a state is safe when the future path seems infinite. In our approach, we always start in the initial state s_0 and assess each state for a possible path in order of preference, hence for any final horizon state we always know that the path leading to state s is finite.

Based on these semantics, we use an LTL property φ for planning, where

$$\varphi = \neg(\text{safe } \mathbf{U} (\text{safe} \wedge \text{horizon})) \quad (13)$$

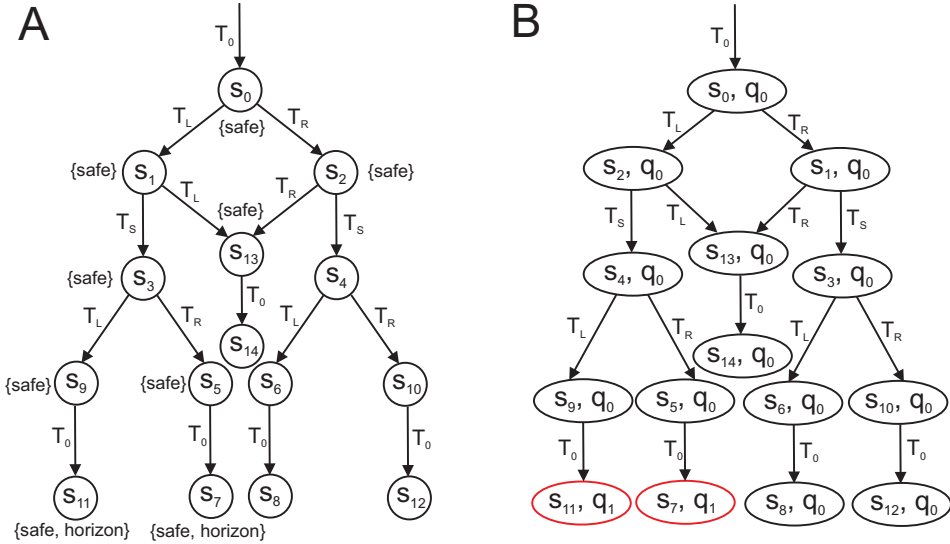
which states that $\neg(\text{safe } \mathbf{U} (\text{safe} \wedge \text{horizon}))$ holds for every path. Note that a finite path satisfies $\text{safe } \mathbf{U} (\text{safe} \wedge \text{horizon})$ if both *safe* and *horizon* are true at some state s in the path, and *safe* is true for all states in the path leading to s . As our interest is in *solution paths* (see Section 3.3), the property φ negates the desired outcome, so that what would normally be the set of counterexamples for a run of the system, in our case becomes a set of safe *future discrete task outcomes*. Consequently, the set of solution paths is the set of paths which satisfy $\text{safe } \mathbf{U} (\text{safe} \wedge \text{horizon})$. Our property and modelling approach is intentionally simple, primarily to ensure fast computation and minimal resource usage for reliability on a low-powered device.

4.4.2 Checking the Product Transition System. The set of counterexamples for φ constitute a language of finite words which can be recognised by an NFA. We therefore construct the NFA


 Fig. 10. NFA for the property $safe \text{ U } (safe \wedge horizon)$.

$\mathcal{A}_{\neg\varphi} = (Q, \Sigma, \delta, Q_0, F)$ where $Q = \{q_0, q_1\}$ is the set of states, $\Sigma = 2^{AP}$ is a finite alphabet, $\delta : Q \times \Sigma \rightarrow 2^Q$ is a transition relation, $Q_0 = \{q_0\}$ is the initial state, and $F = \{q_1\}$ is the accepting state. Figure 10 shows the NFA $\mathcal{A}_{\neg\varphi}$.

When a new disturbance is encountered by the robot, we use the abstraction approach explained in Section 4.2 to assign a valuation to the corresponding state from the set AP . We then calculate the automaton formed as the product of TS and $\mathcal{A}_{\neg\varphi}$ and generate a (finite) accepting path non-deterministically using forward depth-first search (f-DFS). This starts in the root node of the underlying graph (i.e., the initial state s_0) and starts backtracking once a leaf node is reached, which is appropriate as the goal state not determined a priori. From the path we can then extract the transitions to form a plan for the scenario. Figure 11A shows an instance of our transition system with valuation of the elements of $\{horizon, safe\}$ and Figure 11B the product automaton. Note that accepting (solution) paths are those for which the NFA part of the state in Figure 11B is the accepting state q_1 .


 Fig. 11. A: instance of our transition system showing a valuation of the elements of AP . B: product transition system and NFA resulting from the valuation in A.

4.4.3 *Runtime Generation of Plans.* Algorithm 3 provides details on the runtime procedure for computing our abstraction and generating plans. As mentioned above, we assess possible sequences in order of length to determine a valuation of our transition system. Note that the subroutine *generatePlan()* finds a solution path by f-DFS on the product transition system and NFA. Starting from the initial state s_0 , it then extracts the transitions between states form a plan consisting of a sequence of associated tasks. By default f-DFS does not return the accepting state of the product, so the final transition is not returned. However, as the final transition in a plan is always the default task T_0 this is sufficient.

Algorithm 3: Generate Plan Using Model Checking

Input : Set of observations O and disturbance D^+ .

Output : Sequence of discrete control tasks *plan*.

```

1 Procedure GenerateNewPlan( $O, D^+$ )
2    $term \leftarrow \emptyset$  // set of terminal states for product
3    $\Delta^+ \leftarrow \emptyset$  // simulate proximal detection of  $D$ 
4   if  $\Delta^+ > d_{safe}$  then
5      $\Delta^+ = D_x^+ - d_{safe}$ 
6    $O' \leftarrow \emptyset$ 
7   for  $o \in O$  do
8      $o_x \leftarrow o_x - \Delta^+$ 
9     add  $o$  to  $O'$ 
10   $P_L \leftarrow \text{ConstructPY}(O', d_{safe}, d_{max}, \mathbf{true})$  // assess two steps
11   $P_R \leftarrow \text{ConstructPY}(O', d_{safe}, d_{max}, \mathbf{false})$ 
12  if  $P_L = \emptyset$  then
13    add  $s_3$  to  $term$ 
14  if  $P_R = \emptyset$  then
15    add  $s_4$  to  $term$ 
16  if  $P_L = \emptyset \vee P_R = \emptyset$  then
17     $plan \leftarrow \text{generatePlan}(term)$ 
18    return  $plan$  // assess three steps
19  if  $D_y^L \in P_L < d_{min} \wedge D_y^R \in P_R > -d_{min}$  then
20    add  $s_{14}$  to  $term$ 
21     $plan \leftarrow \text{generatePlan}(term)$ 
22    return  $plan$ 
23   $\Delta^L \leftarrow D_y^L - d_{safe}$  // assess four steps
24   $\Delta^R \leftarrow D_y^R + d_{safe}$ 
25   $P_L^+ \leftarrow \text{ConstructPX}(O', \Delta^L, d_{safe}, L + tol, \mathbf{true})$ 
26   $P_L^- \leftarrow \text{ConstructPX}(O', \Delta^L, d_{safe}, L + tol, \mathbf{false})$ 
27   $P_R^+ \leftarrow \text{ConstructPX}(O', \Delta^R, d_{safe}, L + tol, \mathbf{true})$ 
28   $P_R^- \leftarrow \text{ConstructPX}(O', \Delta^R, d_{safe}, L + tol, \mathbf{false})$ 

```

Algorithm 3: (continued)

```

6   if  $P_L^+ = \emptyset$  then
7     |   add  $s_7$  to term
8   if  $P_L^- = \emptyset$  then
9     |   add  $s_{11}$  to term
10  if  $P_R^+ = \emptyset$  then
11    |   add  $s_8$  to term
12  if  $P_R^- = \emptyset$  then
13    |   add  $s_{12}$  to term
14  plan  $\leftarrow$  generatePlan(term)
15  return plan

```

5 DESIGN OF CASE STUDY AND EVALUATION

In this section, we address the research question:

RQ1 Does planning using model checking and closed-loop tasks reliably generate safe obstacle avoidance behaviour?

We aimed to investigate whether planning using model checking and closed-loop tasks reliably generate safe trajectories for obstacle avoidance compared to a reactive agent which can only generate a simple reflex in response to disturbances. In addition, we wanted to demonstrate that multi-step planning means that our approach cannot get trapped in a corner as in single-step planning (see Section 2 for details). We also wanted to gain insight into the reliability of real-time performance with respect to a deadline of 100 milliseconds and investigate the memory usage of model checking.

In Sections 5.1, 5.2 and 5.3 we discuss analysis details for two empirical studies and present results. We provide theoretical results in Section 5.4.

5.1 Artefacts

We used two artefacts in our case study: a baseline method and planning using model checking. Our baseline method was a simple reactive controller which can only spawn a single closed-loop task at a time in response to disturbances, generating stereotyped behaviour for obstacle avoidance.

5.2 Scenario 1 - Cul-de-sac

We initially focused on a cul-de-sac scenario due to the prevalence of corners and parallel walls, as reactive methods for obstacle avoidance based on a single closed-loop controller can easily get trapped in such a situation. Our intention here was to recreate difficulties for the baseline method and see if planning using model checking showed any improvement in behaviour.

5.2.1 Environment Definition. Figure 12A shows three starting positions (“Left”, “Centre”, “Right”) with the orientation of the robot defined relative to the bottom wall. For the centre position, the orientation of the x -axis is offset 0 degrees relative to the bottom wall, but for the left and right starting positions it is offset 45 degrees. There were two reasons for this setup: (i) we wanted to maximise the chances of the baseline method getting trapped, and (ii) pilot experiments revealed that the robot had a strong right veer when driving straight, hence we balanced our study. The

dashed blue line in Figure 12A represents a cut-off used to prepare trajectories for analysis. We collected 15 runs for each method and starting position, resulting in a dataset consisting of 90 runs.

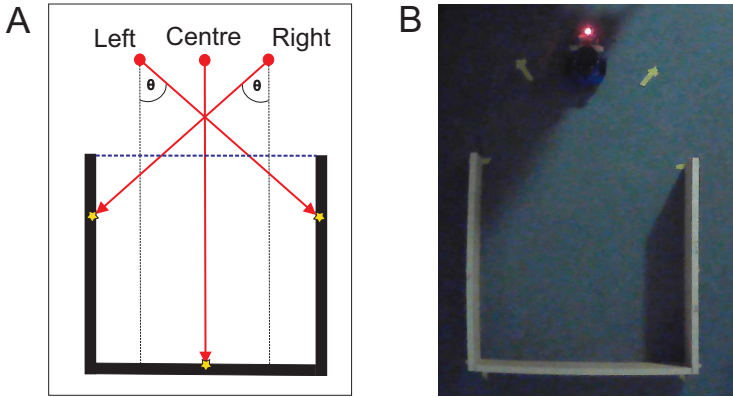


Fig. 12. A: idealised schematic of cul-de-sac scenario. B: actual cul-de-sac scenario.

5.2.2 Analysis of Reliability. We used trajectory length as a proxy for elapsed time to operationalise the construct of reliability, focusing only on the portion of the trajectory in the cul-de-sac (i.e., below the trajectory cut-off in Figure 12A). Our aim was to show statistically that our method spends less time evading the cul-de-sac. In addition, we counted the number of collisions for each method. We also used processing latency as a metric for reliability, defined as the time delta from initiation of planning to completion. We aimed to describe the mean latency and estimate confidence bounds for our method to generate insight into whether our approach can consistently meet real-time constraints.

Design of Analysis. Our study had a 2×3 between-factors design for the statistical analysis of trajectory lengths and reporting of collisions. The method variable had two levels, “Single” and “Multi”, representing the baseline and planning using model checking, respectively. The starting position variable had three levels (“Left”, “Centre”, “Right”) indicated in Figure 12A. We calculated minimum, maximum and mean processing latency for model checking runs and estimated 95% confidence intervals using the bootstrap method.

Data Collection and Preparation. During data collection, we used markers to indicate the correct placement of the robot. Runs were terminated when the robot was observed to pass the threshold of the cul-de-sac by a visibly clear margin. Processing latency was collected for each executed planning sequence at runtime using an in-built time and date package in C++ and the number of collisions was recorded by observation.

In practice, the variation in terminating runs was large, so it made sense to focus only on the portion of the trajectory in the cul-de-sac for the analysis. For each run, we extracted the trajectory from video using the optical flow method in OpenCV⁶ and calculated the length in pixels. Trajectories were truncated at the entrance to the cul-de-sac as shown in Figure 13B.

Results. First we compared trajectory lengths for each method while ignoring starting position. A non-parametric Mann-Whitney U test was performed. As the shape and dispersion of the distributions was different (see Figure 14 for boxplots), the null hypothesis was that the mean ranks

⁶<https://opencv.org/>

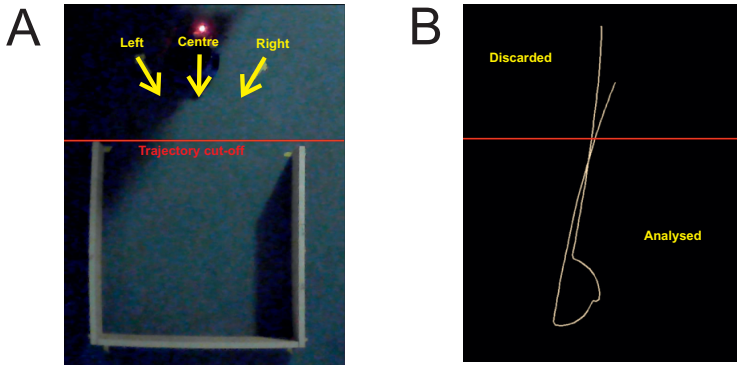


Fig. 13. The experimental setup. A: the three starting positions (left, centre, right) and placement of the trajectory cut-off. B: example trajectory and truncation according to the cut-off in A.

for each method are identical, and the alternative hypothesis was that it is lower for the model checking group, $\alpha = .025$ (one-tailed). The test revealed that the mean rank for model checking was significantly lower, $U = 251, n_1/n_2 = 45, p < .001$, with a medium effect size, $r = .37$.

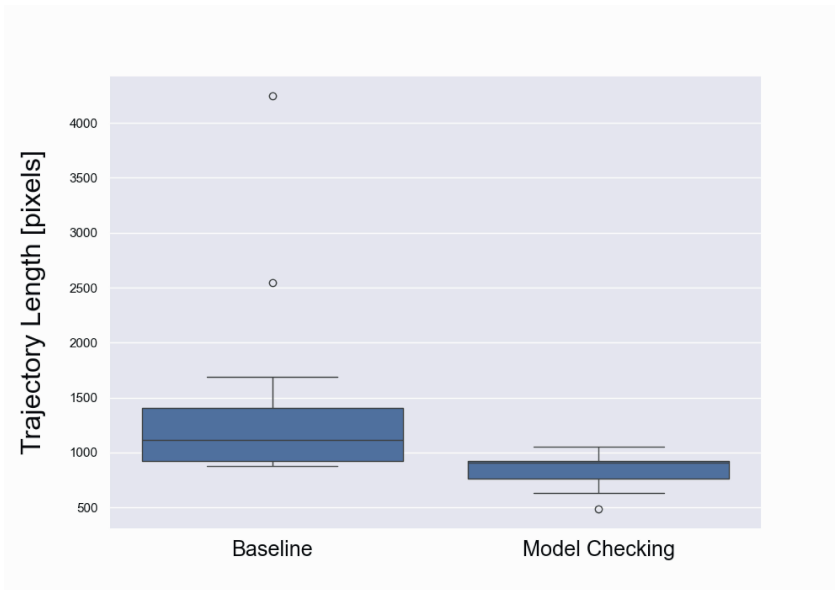


Fig. 14. Trajectory length grouped by method.

Next a comparison was made between starting positions. It was reasoned that this could have an influence on the generated trajectory lengths due to differences in starting pose, specifically angle of entry into the cul-de-sac. We performed a non-parametric Kruskal-Wallis test on starting position and trajectory length for each method individually. For the baseline, the test revealed that there was a significant effect of starting position on trajectory length $H(2) = 12.17, p = .002$. Post-hoc analysis of pairwise comparisons using Dunn’s test (Bonferroni correction applied) revealed that

there was a significant difference between the centre starting position and both the left ($p = .026$) and right ($p = .002$) starting positions, while the left starting position was not significantly different from the right ($p = 1$).⁷ The results suggest the single control task produces similar trajectory lengths when entering the cul-de-sac at an angle of ≈ 45 degrees. See Figure 15A for a comparison of the distributions for each starting position.

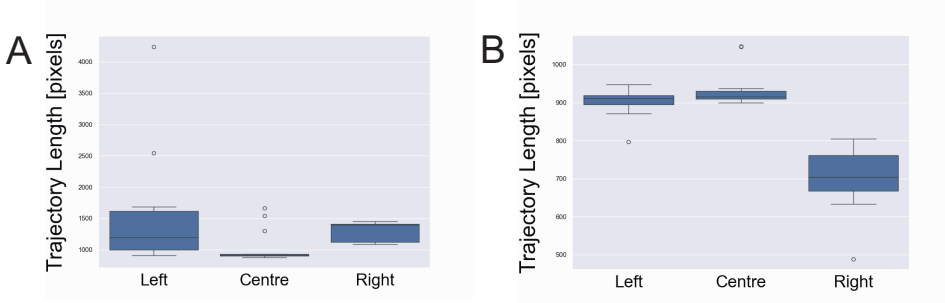


Fig. 15. Trajectory length grouped by starting position. A: baseline, B: model checking.

For the model checking approach, the test also revealed that there was significant effect of starting position $H(2) = 30.2, p < .001$. In this case, post-hoc analysis of pairwise comparisons revealed that there was a significant difference between the centre starting position and the right ($p < .001$) but not the left ($p = .872$), while the left starting position for this method was significantly different from the right ($p < .001$). The results suggest model checking generates different trajectory lengths when entering the cul-de-sac at an angle of ≈ 45 degrees from different starting positions, whereas the centre and left starting positions generate similar trajectory lengths. Figure 15B shows the distributions of trajectory lengths for each starting position.

The number of collisions was also observed for each run. For the baseline method, a total of 3 collisions was observed and 0 collisions were observed for planning using model checking. Note that each collision was observed for a different run of the baseline method (i.e., 3 runs in total). Table 3 shows collisions for the baseline grouped according to starting position.

Table 3. Distribution of collisions for baseline.

Starting position	Collisions
Centre	1
Left	2
Right	0

The minimum processing latency for planning using model checking was 5.58 milliseconds and the maximum was 18.76 milliseconds. The mean was 10.1 milliseconds with an estimated 95% confidence interval of [9.33, 10.96].

5.2.3 Profiling Memory Usage. We focused on *describing* the memory footprint. Memory usage was estimated for both model checking and the entire process. We also estimated process memory usage for the baseline to indicate relative performance.

⁷Rounded down from > 1 , as a secondary effect of the Bonferroni correction.

Design of Analysis. We estimated the runtime memory usage of both model checking and the entire program. Model checking memory usage was estimated by summing the compile time memory of the stack, set and adjacency list data structures used by f-DFS and their worst case usage at runtime, based on a state size of 4 bytes, as each state is represented by an integer.

Data Collection and Preparation. Process memory usage was collected using the Linux top utility at a sampling rate of 1 millisecond. For runtime memory usage of model checking, we recorded the growth of the stack and set of visited states during f-DFS execution and dumped the data to disk.

Results. Maximum memory usage for model checking at runtime was estimated at 2.9 kilobytes, while the maximum memory usage of the process was 4.31 megabytes. However, this includes the amount of shared memory available to a process, not all of which is typically resident to the program (i.e., includes memory which could potentially be shared with other processes). The maximum amount of shared memory was 3.34 megabytes, hence a lower bound on the maximum was calculated at 992 kilobytes. Maximum model checking usage was therefore estimated to comprise 0.06% to 0.29% of maximum process memory usage.

In comparison, maximum process memory usage for the baseline method was 4.3 megabytes with a maximum shared memory component of 3.28 megabytes. In this case, a lower bound on the maximum was calculated at 1.02 megabytes. While there is uncertainty, the data suggests that memory consumption for model checking is approximately equivalent to the baseline.

5.3 Scenario 2 - Playground

We conducted two comparisons between the baseline method and planning using model checking for a playground environment, focusing specifically on evasion of a cul-de-sac element and collisions. Our aim here was to investigate whether our approach showed improvement in obstacle avoidance behaviour during general operation and gain insight into its versatility. We again collected data on real-time performance and profiled memory usage.

5.3.1 Environment Definition. We let the robot roam free in a closed environment with one free-standing static object and a cul-de-sac, as illustrated in Figure 16. We included a cul-de-sac because we were interested in comparing emergent behaviour for each method when negotiating the cul-de-sac during normal operation.

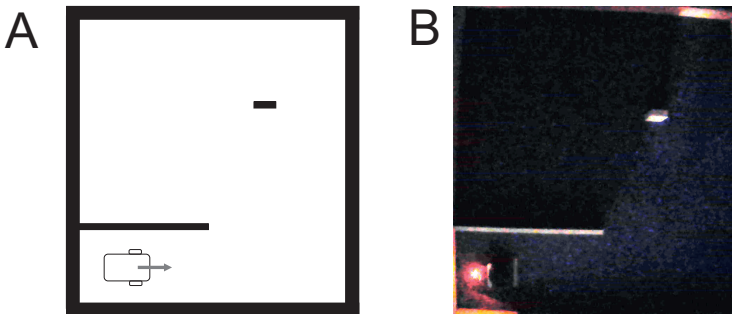


Fig. 16. A: idealised schematic of playground scenario. B: actual playground.

5.3.2 Analysis of Reliability. We used the overall time elapsed inside the cul-de-sac during exploration and processing latency as metrics for reliability. Our aim here was to characterise the relationship between processing latency and plans of different lengths, as it was found in the

previous scenario that only three step plans were generated, introducing bias to the results for real-time performance. In addition, we counted the number of collisions for each run.

Design of Analysis. For each run, we calculated the number of times the cul-de-sac was visited, the time elapsed inside the cul-de-sac and summed the number of collisions. We grouped processing latency by the number of steps in the plan and calculated descriptive statistics, estimating 95% confidence intervals for each plan length.

Data Collection and Preparation. We made two comparisons between the baseline and planing using model checking. For each run, we let the robot explore the playground environment for 5 minutes and recorded the behaviour on video. We then extracted the trajectories using optical flow in OpenCV and inspected the difference visually. Following this, we calculated the number of times the robot visited the cul-de-sac and time elapsed inside the cul-de-sac, using the light on the robot as a point of reference for consistency with analysis of the previous scenario. We also considered the cul-de-sac visited if the robot manoeuvred to evade. Following the same protocol of the previous scenario, we recorded the number of collisions for each run. Data collection and preparation was the same as in the previous scenario for processing latency. We also extracted the number of steps for each plan.

Results. Figure 17 shows extracted trajectories for the first comparison. It can be seen in Figure 17A (baseline) that the robot spends significant time in the cul-de-sac, whereas in Figure 17B (planning using model checking) the robot spends no time in the cul-de-sac. The baseline method visited the cul-de-sac once during the run at which point it got trapped for 89 seconds. There were 4 collisions for the baseline and 0 collisions for model checking.

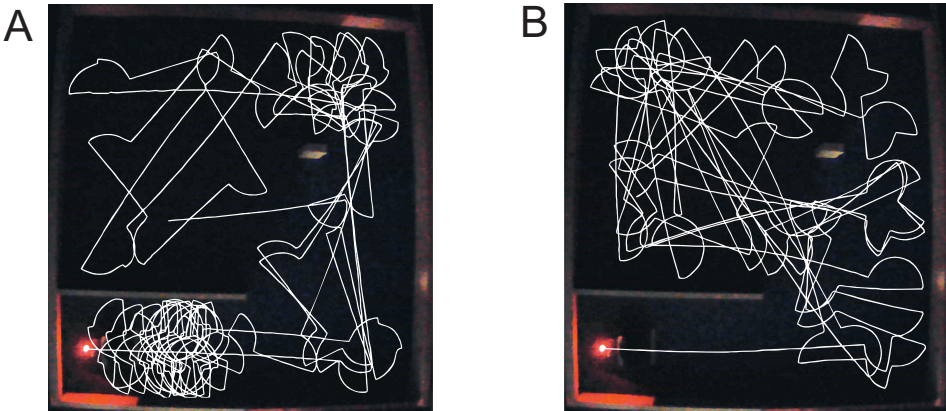


Fig. 17. Comparison 1. A: baseline method. B: planning using model checking.

In Figure 18 trajectories for the second comparison are shown. Figure 18A shows that the baseline method spends significant time in the cul-de-sac. However, in this case, the robot visited the cul-de-sac on three separate occasions for a total elapsed time of 79 seconds. For this comparison, planning using model checking also visited the cul-de-sac on three separate occasions but evaded rather than enter the cul-de-sac. The total time elapsed for evasion was 12 seconds. Evasion manoeuvres are indicated by the yellow box in Figure 18B. On one occasion, the robot had to execute three consecutive two step plans before a successful evasion of the cul-de-sac, indicating the possibility that there may be scenarios where the robot can still get trapped. There were 2 collisions for the baseline and 0 collisions for model checking.

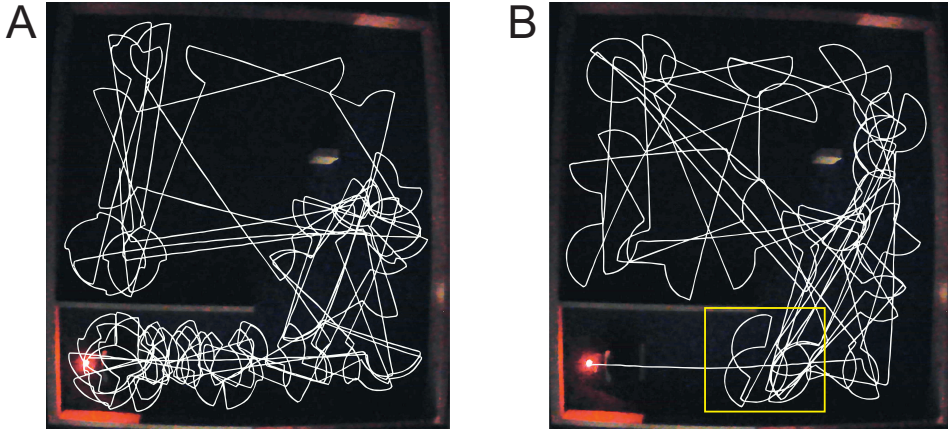


Fig. 18. Comparison 2. A: baseline method. B: planning using model checking (yellow box indicates evasion manoeuvres at entrance to the cul-de-sac).

Table 4 shows results for processing latency across both model checking runs grouped according to the number of steps in plans. There were 42 two step plans, 32 three step plans and 18 four step plans. Processing latency appears to increase as the length of the plan increases.

Table 4. Processing latency in milliseconds for plans consisting of 2, 3 and 4 steps.

Steps(n)	Min.	Max.	Mean	CI (95%)
2	2.5	14.09	6.64	[5.92, 7.44]
3	5.12	12.15	7.66	[7.11, 8.35]
4	5.45	21.61	11.49	[9.6, 13.83]

5.3.3 Profiling Memory Usage. Memory usage was estimated for model checking and the entire process. We again estimated process memory usage for the baseline method to provide an indicative comparison of relative resource usage. Analysis design and data collection/preparation were the same as in the previous scenario.

Results. Maximum memory usage by model checking at runtime was estimated at 2.91 kilobytes and maximum memory usage of the process at 4.09 megabytes. Again this includes the amount of shared memory available to a process, which could potentially be shared with other processes. The maximum amount of shared memory was 3.03 megabytes, hence a lower bound on the maximum was calculated at 1088 kilobytes. Maximum model checking memory usage was estimated to comprise 0.06% to 0.26% of maximum process memory usage.

In comparison, maximum process memory usage for the baseline was 3.83 megabytes with a maximum shared memory component of 2.95 megabytes. A lower bound on the maximum was calculated at 900 kilobytes. As in the previous scenario, the data suggests that process memory consumption is approximately equivalent for each method.

5.4 Theoretical Results

In this section, we provide informal proofs of two fundamental properties of our approach. Specifically, we show that for any arbitrary static environment: (i) the robot cannot get trapped in a corner, and (ii) no disturbance can enter the safe zone, as long as the parameters for our abstraction meet certain criteria.

5.4.1 Corner Scenarios. One of the main drawbacks of the baseline method is the potential for the robot to get trapped in a corner, as explained in Section 2. For this reason, we compared our method to the baseline method in a close study of a cul-de-sac scenario with two corners (see Section 5.2 for details).

A generic definition of “getting trapped” is that the robot executes a repeating sequence of tasks which results in the robot visiting the same configurations in a loop. Getting trapped in a corner is one specific instance of this behaviour, defined here as the robot alternating between tasks T_L and T_R . We now show that this cannot happen using our approach.

THEOREM 5.1. *Let $\mathcal{T} = T_0T_1T_2 \dots$ be a sequence of tasks from the set $Act = \{T_L, T_R, T_S, T_0\}$ executed for an infinite run of the robot. Then there is no subsequence of tasks in \mathcal{T} which alternates between tasks T_L and T_R .*

PROOF. Assume there is a subsequence in \mathcal{T} which alternates between T_L and T_R . Then \mathcal{T} contains at least the ordered pair $\langle T_L, T_R \rangle$ or $\langle T_R, T_L \rangle$. By definition, no path in the disturbance-focused transition system DTS contains $\langle T_L, T_R \rangle$ or $\langle T_R, T_L \rangle$, so no subsequence of tasks generated as a plan can contain a subsequence which alternates between tasks T_L and T_R . As the last task in a plan is always the default task T_0 , it is not possible for the last and first task of consecutive plans to form the pair $\langle T_L, T_R \rangle$ or $\langle T_R, T_L \rangle$. There is no other way that the pairs can be formed. Hence a subsequence in \mathcal{T} cannot alternate between T_L and T_R which contradicts our assumption. \square

While it is guaranteed that our approach cannot get trapped in a corner, it is nonetheless possible for the robot to get trapped in other ways. For example, in some environments the robot could get stuck in a loop by always turning left/right then driving straight, either by repeatedly executing two step or four step plans. Depending on the angle of the initial disturbance, it is also possible for the robot to get trapped between parallel walls by executing three step plans repeatedly. However, this is contingent on the distance between parallel walls relative to the parameters of the abstraction. All these situations are unlikely to happen in practice but theoretically possible.

5.4.2 Safe Zone. Our use of a safe zone around the robot mitigates the need for a formal guarantee that our abstraction preserves safety for an avoid task (i.e., a rotation), as indicated in Section 4.2.1. The safe zone is defined as a circle around the centre of mass of the robot, however in practice we over-approximate the safe zone using a square construction. This is defined as the partition:

$$P_{safe} = \{0 \in O \mid 0 < |o_x| \leq d_{safe} \wedge 0 < |o_y| \leq d_{safe}\} \quad (14)$$

where 0 indicates the origin of the point cloud, which in the real world correlates with the centre of mass, and d_{safe} is the radius of the safe zone.

As mentioned in Section 4.2.1, if the robot is executing the default task T_0 and a disturbance D^+ is witnessed in partition P_{look} , then a new plan is generated using model checking. The robot then continues driving straight in task T_S until the disturbance is witnessed in partition P_{shield} at which point the first task in the plan is initiated. If the task T_S is an intermediate task in a four step plan, then the next task in the plan is initiated when a disturbance is witnessed in P_{shield} . As an additional fail safe, the robot stops if a disturbance is witnessed in partition P_{shield} and no plan is available.

To ensure action is always taken to prevent a disturbance from entering the safe zone, we require that the shield partition be defined as:

$$P_{shield} = \{o \in O \mid d_{safe} < \min(o_x) \leq v\Delta t + \epsilon \wedge |o_y| \leq \frac{1}{2}(L + tol)\} \quad (15)$$

where d_{safe} is again the radius of the safe zone, $v\Delta t$ is the predicted distance the robot will travel in one closed-loop step, ϵ is the negative or positive error between the actual and predicted distance, and $\frac{1}{2}(L + tol)$ defines the width of the partition in the lateral dimension. We in addition require that $\frac{1}{2}(L + tol) = d_{safe}$ to focus attention on relevant future disturbances.

Based on the parameters defined for P_{safe} and P_{shield} , we now show that no disturbance can enter the safe zone when executing a straight task. It is sufficient to show that this cannot happen for a single closed-loop step. As Δt is around 200 milliseconds, we assume any lateral error is negligible.

THEOREM 5.2. *Let $O = \dots O(t-2)O(t-1)O(t)$ be a time series of sets of observations for each closed-loop step during an infinite run of the robot. Then for any set of observations $O(t)$ during execution of a straight task it is guaranteed that a disturbance D^+ cannot be witnessed in the safe zone P_{safe} .*

PROOF. Assume that during execution of a straight task a disturbance is witnessed in the safe zone, hence $D^+ \in O(t)$ and $D^+ \in P_{safe}$. Then this means that in the previous time step $D^+ \in O(t-1)$ and $D^+ \notin P_{shield}$. As the lateral dimension of P_{shield} is equal to the width of P_{safe} , and the lateral error is assumed zero, it is guaranteed that $D_y^+ \in P_{shield}$ for set $O(t-1)$. Hence the inequality $D_x^+ > d_{safe} + v\Delta t + \epsilon$ must hold by the definition of P_{shield} in Equation 15. As the robot drives straight distance $v\Delta t + \epsilon$ between sets of observations, we therefore have the inequality $D_x^+ - v\Delta t + \epsilon > d_{safe}$ for the set of observations $O(t)$. By the definition of P_{safe} in Equation 14, this means $D^+ \in O(t)$ and $D^+ \notin P_{safe}$ which contradicts our assumption. Hence a disturbance cannot be witnessed in the safe zone during a straight task. \square

In practice, this result means that the longitudinal dimension of P_{shield} should scale in proportion to the velocity of the robot. However, the error term ϵ is impossible to predict, so the most sensible strategy is to over-approximate a positive error using a fixed tolerance $v\Delta t + tol$. If the error term ϵ is negative, then it is guaranteed that a disturbance will be witnessed in P_{shield} . If it is positive, then as long as tol is at least equal to the error term, it is also guaranteed that a disturbance will be witnessed in P_{shield} .

5.5 Summary

In Scenario 1 we conducted a close study of a cul-de-sac. We compared trajectory lengths and collisions for a baseline and planning using model checking and found evidence that model checking reliably produces more efficient trajectories for avoiding a cul-de-sac. There were 3 collisions for the baseline method and 0 for model checking, however we had no data on emergent behaviour under general operation of the robot. We also collected data on the processing latency of our approach. Processing latency was well within the 100 milliseconds real-time deadline. However, we found that the nature of the cul-de-sac setup had side effects which restricted the generality of our conclusions—only three step plans were generated, so we had no data on the range of plan lengths. We also profiled memory usage. While direct comparisons were not supported by the data, it was indicated that planning using model checking used similar memory resources to the baseline method.

In Scenario 2 we let the robot roam free in a playground environment. We compared time spent in the cul-de-sac and the number of collisions. In both comparisons, the robot spent a significant

amount of time in the cul-de-sac using the baseline method but none using our approach. There were 6 collisions for the baseline method and 0 for planning using model checking. In addition, we collected data on processing latency and grouped it according to the plan length. We observed an increase in mean processing latency associated with an increase in plan length, however the maximum latency was 21.61 milliseconds, again well within the 100 milliseconds deadline. We again profiled memory usage which was similar to the cul-de-sac scenario.

Finally, we presented two theoretical results which guarantee that with our approach (i) the robot cannot get trapped in a corner scenario (in contrast to the baseline method) and (ii) that collision free navigation is guaranteed.

6 DISCUSSION

We have addressed **RQ1** and shown that a bespoke implementation of model checking can be used to reliably plan sequences of closed-loop tasks for efficient obstacle avoidance on a low-powered autonomous robot. In contrast to a baseline method, which is based on a single control loop, our application of real-time model checking reliably avoids collisions and is not prone to getting trapped in a cul-de-sac. Our approach achieved a processing latency within hard real-time constraints and used minimal additional memory.

There have been notable implementations of real-time model checking for planning on autonomous systems. In [37] an approach for *online strategy synthesis* was developed to derive action plans with formal safety guarantees for steerable needles implemented using the UPPAAL STRATEGO [15] model checker and Python. Plan synthesis took between 0.04 and 6.99 seconds. Our approach was reliably faster as we did not use an off-the-shelf model checker, hence it was possible to optimise our approach for real-time. Standard model checkers include additional functionality leading to a bloated system appropriate for offline verification but sub-optimal for online planning tasks, especially on a resource-constrained device. Indeed, this issue was encountered in [48], where time lag due to model compilation (approx. 3 seconds) made using the SPIN model checker for real-time planning on a real autonomous robot infeasible, particularly in high speed contexts [40].

In addition, the environment in [37] was structured and fully observable, however this assumption is often unrealistic in navigation for autonomous robots [46]. Driving in the real world, for example, is a broad activity domain in which it is impossible for developers to foresee all future situations [12]. While a high definition map is often used in AV prototypes, they are notoriously difficult to maintain and imprecise in complex driving conditions [62]. Hence in SAE level 5 autonomous driving (i.e., full automation requiring no human oversight) an AI-enabled driving system should be able to adapt to unpredictable situations based on egocentric sensory inputs. This requires the ability to understand and interpret structural information about the environment and reason flexibly about possible courses of action which our approach does.

In comparison, deep learning approaches for autonomous navigation in mobile robots, such as deep reinforcement learning (DRL), learn rigid generalisations from data [56] which ignores structural information from the immediate environment vital for reactive obstacle avoidance. While deep neural network approaches are attractive due to the possibility of doing end-to-end learning (i.e., learning optimal actions based on sensor data), even simple models require large amounts of training data, and yet they are still prone to error in unstructured environments. In autonomous driving, the generalisation error of popular DRL approaches is further compounded by the so-called “reality gap” [11, 31]. For ethical reasons models are trained offline in simulated environments, which generates large amounts of training data but ultimately cannot replicate real world driving conditions. The result is a model which serves predictions in real-time but makes opaque decisions insensitive to the local environment, increasing the risk of collisions.

Online methods using symbolic representations, such as our approach using model checking, can potentially offer a route to flexible general reasoning for partially observed, unstructured environments which is safe, reliable and explainable. However, real-time performance is crucial, particularly for high speed driving scenarios. It has been argued that even a lag of 100 milliseconds is unacceptable [40, 42]. While real-time obstacle avoidance for a robot in partially observed and unstructured environments was investigated in [7], the approach can only reason about the current trajectory to ensure the robot is at rest for imminent collisions, hence no planning is involved. Real-time performance was reported at 49 milliseconds via simulation on an average laptop. In comparison, our approach achieves real-time planning with a processing latency less than 22 milliseconds on a low-powered robot.

The inability to plan is a general limitation of runtime verification methods, which typically synthesise a monitor to flag unwanted behaviour during execution and potentially trigger remedial action. In [17], for example, drones were simulated offline, plans generated by conventional means, and runtime monitors synthesised using model checking to ensure model properties are satisfied during execution. Both [49] and [43] synthesised a safety monitor as an extra layer between the motion planner and trajectory tracker to check if trajectories generated by the planner violated certain criteria. In [13] a monitor was synthesised based on verified models of a quadcopter flight controller to trigger corrective action (e.g., emergency landing). In contrast, we perform planning with the model checker itself instead of checking if an existing algorithm leads to a dangerous situation [25]. We define a robot safe zone to ensure our approach does not lead to collisions during execution.

Planning algorithms often assume that a robot moves in a global coordinate system in which trajectories are generated as continuous or piecewise continuous curves. In this context, model checking can be performed offline to synthesise a runtime monitor for the trajectory following error and signal fatal deviations [41], effectively performing classical line following. However, converting a local coordinate system into global coordinates from unreliable sensor data is non-trivial [38, 54] and hard to achieve in real-time without precise offline map data. In [49], for example, a cleaned and labelled global map is used to check generated trajectories for potential violations, and in [43] the locations of pedestrians in global coordinates are simulated. In contrast, we take a constructivist [51] approach and keep the environment partially observable by only working with sensory inputs that are accessible from an egocentric perspective, i.e., the relative position of disturbances. We do not need a global perspective on the robot as we do not perform precise line following along a globally defined trajectory. Instead, closed-loop tasks have an attentional focus on a specific disturbance which they need to counteract.

An obvious limitation of our approach is that obstacle avoidance is not target-driven. However, any realistic task involving autonomous navigation, such as overtaking for AVs, will require target-driven behaviour. To achieve this, some form of localisation in the environment is required, usually through Simultaneous Localisation and Mapping techniques (SLAM) [53]. However, this approach can be computationally expensive—performance of the localisation operation alone can impose a lag in the order of hundreds of milliseconds [6, 39] on the planning process. While sensor fusion techniques may achieve even more precise localisation [63], time performance is seldom measured, and experimental validation often utilises more powerful processors than is available on a Raspberry Pi (e.g., [50, 60]). While localisation is clearly important for a complete robotic system, our focus is on flexible decision making. Hence we have deliberately omitted localisation from our initial investigation into the use of model checking for real-time obstacle avoidance.

A drawback of our current approach is that the development of our real-time model checker was for a specific hardware platform (i.e., Alphasbot with 2D LiDAR and a differential drive), which could be addressed in the future by developing a resource-efficient stand alone model checker optimised

for real-time planning. This would allow the development of models offline using automated tools, perhaps even using some visual syntax (e.g., similar to Traffic Sequence Charts [14] for autonomous driving applications) to increase accessibility for developers without expertise in model checking. Our approach is optimised for real-time as a first step in this direction.

As an explainable method, we believe our approach shows promise as an avenue for the development of safe and reliable decision-making for AVs. In addition, formal verification techniques for hybrid systems could potentially be integrated with our planning approach to provide safety guarantees on behaviour at design time. In [33], for example, vehicle platooning is represented as a multi-agent system using the GWENDOLEN agent programming language. Verification is modularised using Agent Java Pathfinder (AJPF) [16] for discrete decision-making and the UPPAAL model checker [28] for continuous real-time requirements. A similar approach is used to verify the behaviour of a rational agent acting as decision-maker for an AV in [20]. In general, verification of hybrid systems is difficult. However, a modular approach combined with the use of “core” knowledge may simplify the effort.

7 CONCLUSION

We have demonstrated how model checking can be used to generate sequences of closed-loop tasks for real-time obstacle avoidance *in situ* on a low-powered robotic agent. Abstraction is used to represent the temporal evolution of closed-loop tasks as static geometric relationships and facilitate reasoning about discrete task outcomes. This motivated the definition of a finite transition system describing possible robot behaviour which receives a valuation of atomic propositions at runtime. We used a regular LTL property for specifying plans, where a plan is a path in the transition system satisfying the negation of a given property. We have explained how the planning procedure reasons about the safety of possible task sequences and implements a bias towards selecting the shortest without consecutive avoid tasks. We have demonstrated in a case study that our approach is able to generate efficient obstacle avoidance behaviour compared to a simple reactive baseline, well within hard real-time constraints. In addition, we have provided informal proofs of two fundamental properties of our approach: that the robot cannot get trapped in a corner scenario, and that collisions are always avoided.

Our approach is a successful first step towards the use of model checking for real-time planning. The main benefit of our approach is the ability to reason flexibly about the immediate environment based on egocentric sensory inputs, making it reactive to structural information necessary for avoiding imminent collisions. In future work, we intend to extend our approach to accommodate target-driven behaviour while continuing to meet hard real-time constraints. We believe that our approach using model checking shows promise as an avenue for the development of safe, reliable and explainable decision-making for autonomous vehicles which is also energy efficient.

ACKNOWLEDGMENTS

For the purpose of open access, the author(s) has applied a Creative Commons Attribution (CC BY) licence to any Author Accepted Manuscript version arising from this submission.

This work was supported by a grant from the UKRI Strategic Priorities Fund to the UKRI Research Council [EP/V026607/1]; the UKRI Centre for Doctoral Training in Socially Intelligent Artificial Agents [EP/S02266X/1]; and the UKRI Engineering and Physical Sciences Research Council Doctoral Training Partnership award [EP/T517896/1-312561-05].

REFERENCES

- [1] Rajeev Alur, Costas Courcoubetis, and David Dill. 1990. Model-checking for real-time systems. In *[1990] Proceedings. Fifth Annual IEEE Symposium on Logic in Computer Science*. IEEE, 414–425. doi:10.1109/LICS.1990.113766

- [2] Christel Baier and Joost-Pieter Katoen. 2008. *Principles Of Model Checking*. Vol. 950. The MIT Press, Cambridge, Mass. doi:10.1093/comjnl/bxp025 Publication Title: MIT Press ISSN: 00155713.
- [3] Davide Basile, Alessandro Fantechi, and Irene Rosadi. 2021. Formal Analysis of the UNISIG Safety Application Intermediate Sub-layer. In *Formal Methods for Industrial Critical Systems*, Alberto Lluch Lafuente and Anastasia Mavridou (Eds.). Springer International Publishing, Cham, 174–190.
- [4] Peter W. Battaglia, Jessica B. Hamrick, and Joshua B. Tenenbaum. 2013. Simulation as an engine of physical scene understanding. *Proceedings of the National Academy of Sciences* 110, 45 (2013), 18327–18332. doi:10.1073/pnas.1306572110 arXiv:https://www.pnas.org/doi/pdf/10.1073/pnas.1306572110
- [5] Rose Bohrer, Yong Kiam Tan, Stefan Mitsch, Magnus O. Myreen, and André Platzer. 2018. VeriPhy: verified controller executables from verified cyber-physical system models. *SIGPLAN Not.* 53, 4 (June 2018), 617–630. doi:10.1145/3296979.3192406
- [6] Sara Bouraine, Abdelhak Bougouffa, and Ouahiba Azouaoui. 2022. Particle swarm optimization for solving a scan-matching problem based on the normal distributions transform. *Evolutionary Intelligence* 15, 1 (3 2022), 683–694. doi:10.1007/S12065-020-00545-Y/FIGURES/8
- [7] Sara Bouraine, Thierry Fraichard, and Hassen Salhi. 2012. Provably safe navigation for mobile robots with limited field-of-views in dynamic environments. *Autonomous Robots* 32, 3 (01 Apr 2012), 267–283. doi:10.1007/s10514-011-9258-8
- [8] V. Braitenberg. 1986. *Vehicles: Experiments in Synthetic Psychology*. MIT Press, Cambridge, Massachusetts.
- [9] R. C. Cardoso, G. Kourtis, L. A. Dennis, C. Dixon, M. Farrell, M. Fisher, and M. Webster. 2021. A Review of Verification and Validation for Space Autonomous Systems. *Current Robotics Reports* 2, 3 (2021), 273–283. doi:10.1007/s43154-021-00058-1
- [10] Christopher Chandler, Bernd Porr, Alice Miller, and Giulia Lafratta. 2023. Model Checking for Closed-Loop Robot Reactive Planning. *Electronic Proceedings in Theoretical Computer Science* 395 (Nov. 2023), 77–94. doi:10.4204/eptcs.395.6
- [11] Li Chen, Penghao Wu, Kashyap Chitta, Bernhard Jaeger, Andreas Geiger, and Hongyang Li. 2024. End-to-End Autonomous Driving: Challenges and Frontiers. *IEEE Transactions on Pattern Analysis and Machine Intelligence* 46, 12 (2024), 10164–10183. doi:10.1109/TPAMI.2024.3435937
- [12] François Chollet. 2019. On the Measure of Intelligence. doi:10.48550/arXiv.1911.01547 arXiv:1911.01547 [cs]
- [13] Silvano Dal Zilio, Pierre-Emmanuel Hladik, Félix Ingrand, and Anthony Mallet. 2023. A formal toolchain for offline and run-time verification of robotic systems. *Robotics and Autonomous Systems* 159 (2023), 104301. doi:10.1016/j.robot.2022.104301
- [14] Werner Damm, Eike Möhlmann, Thomas Peikenkamp, and Astrid Rakow. 2018. A Formal Semantics for Traffic Sequence Charts. In *Principles of Modeling*, Marten Lohstroh, Patricia Derler, and Marjan Sirjani (Eds.). Vol. 10760. Springer International Publishing, 182–205. doi:10.1007/978-3-319-95246-8_11 Series Title: Lecture Notes in Computer Science.
- [15] Alexandre David, Peter Gjøøl Jensen, Kim Guldstrand Larsen, Marius Mikućionis, and Jakob Haahr Taankvist. 2015. Uppaal Stratego. In *Tools and Algorithms for the Construction and Analysis of Systems*, Christel Baier and Cesare Tinelli (Eds.). Vol. 9035. Springer Berlin Heidelberg, 206–211. doi:10.1007/978-3-662-46681-0_16 Series Title: Lecture Notes in Computer Science.
- [16] Louise A. Dennis, Michael Fisher, Matthew P. Webster, and Rafael H. Bordini. 2012. Model checking agent programming languages. *Automated Software Engineering* 19, 1 (March 2012), 5–63. doi:10.1007/s10515-011-0088-x
- [17] Ankush Desai, Tommaso Dreossi, and Sanjit A. Seshia. 2017. Combining Model Checking and Runtime Verification for Safe Robotics. In *Runtime Verification*, Shuvendu Lahiri and Giles Reger (Eds.). Springer International Publishing, Cham, 172–189.
- [18] European Commission. Joint Research Centre. 2021. Trustworthy autonomous vehicles: assessment criteria for trustworthy AI in the autonomous driving domain. <https://data.europa.eu/doi/10.2760/120385>
- [19] Marie Farrell and Matt Luckcuck (Eds.). 2021. *Proceedings of the Third Workshop on Formal Methods for Autonomous Systems*. Vol. 348. Open Publishing Association. doi:10.4204/eptcs.348
- [20] L. E. R. Fernandes, V. Custodio, G. V. Alves, and M. Fisher. 2017. A Rational Agent Controlling an Autonomous Vehicle: Implementation and Formal Verification. *Electronic Proceedings in Theoretical Computer Science* 257 (2017), 35–42. doi:10.1007/978-94-015-9204-8
- [21] Angelo Ferrando, Rafael C. Cardoso, Michael Fisher, Davide Ancona, Luca Franceschini, and Viviana Mascardi. 2020. ROSMonitoring: A Runtime Verification Framework for ROS. In *Towards Autonomous Robotic Systems: 21st Annual Conference, TAROS 2020, Nottingham, UK, September 16, 2020, Proceedings* (Nottingham, United Kingdom). Springer-Verlag, Berlin, Heidelberg, 387–399. doi:10.1007/978-3-030-63486-5_40
- [22] Angelo Ferrando, Louise A. Dennis, Davide Ancona, Michael Fisher, and Viviana Mascardi. 2018. Verifying and Validating Autonomous Systems: Towards an Integrated Approach. In *Runtime Verification*, Christian Colombo and Martin Leucker (Eds.). Springer International Publishing, Cham, 263–281.

- [23] Mohammed Foughali, Saddek Bensalem, Jacques Combaz, and Félix Ingrand. 2020. Runtime Verification of Timed Properties in Autonomous Robots. In *2020 18th ACM-IEEE International Conference on Formal Methods and Models for System Design (MEMOCODE)*. 1–12. doi:10.1109/MEMOCODE51338.2020.9315156
- [24] D. Fraser, R. Giaquinta, Hoffmann, M. Ireland, A. Miller, and G. Norman. 2020. Collaborative models for autonomous systems controller synthesis. *Form Aspects of Computing* 32 (2020), 157–186. doi:10.1109/TCST.2006.872519
- [25] Rong Gu, Cristina Seceleanu, Eduard Enoiu, and Kristina Lundqvist. 2021. Model Checking Collision Avoidance of Nonlinear Autonomous Vehicles. In *Formal Methods*, Marieke Huisman, Corina Păsăreanu, and Naijun Zhan (Eds.). Springer International Publishing, Cham, 676–694.
- [26] J. Hamilton, I. Stefanakos, R. Calinescu, and J. Cámara. 2022. Towards Adaptive Planning of Assistive-care Robot Tasks. In *Electronic Proceedings in Theoretical Computer Science*, Matt Luckcuck and Marie Farrell (Eds.), Vol. 371. Open Publishing Association, 175–183. doi:10.4204/eptcs.371
- [27] K. Havelund, M. Lowry, and J. Penix. 2001. Formal Analysis of a Space-Craft Controller Using SPIN. *Software Engineering, IEEE Transactions on* 27 (09 2001), 749–765. doi:10.1109/32.940728
- [28] M. Hendriks, P. Petterson, J. Hakansson, K.G. Larsen, A. David, G. Behrmann, Wang Yi, P. Petterson, J. Hakansson, K.G. Larsen, A. David, G. Behrmann, M. Hendriks, and Wang Yi. 2006. UPPAAL 4.0. In *Third International Conference on the Quantitative Evaluation of Systems - (QEST'06)*. IEEE, Riverside, CA, 125–126. doi:10.1109/QEST.2006.59
- [29] Thomas A. Henzinger, Pei-Hsin Ho, and Howard Wong-Toi. 1997. HyTech: A model checker for hybrid systems. In *Computer Aided Verification*, Orna Grumberg (Ed.). Springer Berlin Heidelberg, Berlin, Heidelberg, 460–463.
- [30] G. Holzmann. 2011. *The SPIN Model Checker: Primer and Reference Manual* (1st ed.). Addison-Wesley Professional.
- [31] Xuemin Hu, Shen Li, Tingyu Huang, Bo Tang, Rouxing Huai, and Long Chen. 2023. How Simulation Helps Autonomous Driving: A Survey of Sim2real, Digital Twins, and Parallel Intelligence. doi:10.48550/arXiv.2305.01263 arXiv:2305.01263 [cs]
- [32] Jeff Huang, Cansu Erdogan, Yi Zhang, Brandon Moore, Qingzhou Luo, Aravind Sundaresan, and Grigore Rosu. 2014. ROSRV: Runtime Verification for Robots. In *Runtime Verification*, Borzoo Bonakdarpour and Scott A. Smolka (Eds.). Springer International Publishing, 247–254.
- [33] Maryam Kamali, Louise A. Dennis, Owen McAree, Michael Fisher, and Sandor M. Veres. 2017. Formal verification of autonomous vehicle platooning. *Science of Computer Programming* 148 (2017), 88–106. doi:10.1016/j.scico.2017.05.006 Special issue on Automated Verification of Critical Systems (AVoCS 2015).
- [34] Giulia Lafratta, Bernd Porr, Christopher Chandler, and Alice Miller. 2025. Closed-loop multi-step planning. *Neural Computation* (forthcoming) (2025).
- [35] Brenden M. Lake, Tomer D. Ullman, Joshua B. Tenenbaum, and Samuel J. Gershman. 2017. Building machines that learn and think like people. *Behavioral and Brain Sciences* 40 (2017), e253. doi:10.1017/S0140525X16001837
- [36] Yann LeCun. 2022. A Path Towards Autonomous Machine Intelligence | OpenReview. <https://openreview.net/forum?id=BZ5a1r-kVsf>
- [37] S. Lehmann, A. Rogalla, M. Neidhardt, A. Schlaefler, and S. Schupp. 2021. Online Strategy Synthesis for Safe and Optimized Control of Steerable Needles, See [19], 128–135. doi:10.4204/EPTCS.348.9
- [38] J.J. Leonard and H.F. Durrant-Whyte. 1991. Simultaneous map building and localization for an autonomous mobile robot. In *Proceedings IROS '91:IEEE/RSJ International Workshop on Intelligent Robots and Systems '91*. 1442–1447 vol.3. doi:10.1109/IROS.1991.174711
- [39] Bo Li, Yingqiang Wang, Yu Zhang, Wenjie Zhao, Jianyuan Ruan, and Ping Li. 2020. GP-SLAM: laser-based SLAM approach based on regionalized Gaussian process map reconstruction. *Autonomous Robots* 44, 6 (7 2020), 947–967. doi:10.1007/S10514-020-09906-Z/FIGURES/26
- [40] Xiaohui Li, Zhenping Sun, Dongpu Cao, Zhen He, and Qi Zhu. 2016. Real-Time Trajectory Planning for Autonomous Urban Driving: Framework, Algorithms, and Verifications. *IEEE/ASME Transactions on Mechatronics* 21, 2 (April 2016), 740–753. doi:10.1109/TMECH.2015.2493980
- [41] Qin Lin, Stefan Mitsch, André Platzer, and John M. Dolan. 2022. Safe and Resilient Practical Waypoint-Following for Autonomous Vehicles. *IEEE Control Systems Letters* 6 (2022), 1574–1579. doi:10.1109/LCSYS.2021.3125717
- [42] Shih-Chieh Lin, Yunqi Zhang, Chang-Hong Hsu, Matt Skach, Md E. Haque, Lingjia Tang, and Jason Mars. 2018. The Architectural Implications of Autonomous Driving: Constraints and Acceleration. In *Proceedings of the Twenty-Third International Conference on Architectural Support for Programming Languages and Operating Systems* (Williamsburg VA USA, 2018-03-19). ACM, 751–766. doi:10.1145/3173162.3173191
- [43] Stefan B. Liu, Hendrik Roehm, Christian Heinzemann, Ingo Lütkebohle, Jens Oehlerking, and Matthias Althoff. 2017. Provably safe motion of mobile robots in human environments. In *2017 IEEE/RSJ International Conference on Intelligent Robots and Systems (IROS)*. 1351–1357. doi:10.1109/IROS.2017.8202313
- [44] Dennis Louise, Michael Fisher, Nicholas Lincoln, Alexei Lisitsa, and Sandor Veres. 2016. Practical verification of decision-making in agent-based autonomous systems. *Automated Software Engineering* 23, 3 (2016), 305–359. doi:10.1007/s10515-014-0168-9

- [45] Y. Lu, A. Miller, C. Johnson, Z. Peng, and T. Zhao. 2014. Availability analysis of satellite positioning systems for aviation using the Prism model checker. In *Proceedings of the 17th International Conference on Computational Science and Engineering (CSE 2014)*. 704–713. doi:10.1109/CSE.2014.148
- [46] Matt Luckcuck, Marie Farrell, Louise A. Dennis, Clare Dixon, and Michael Fisher. 2019. A Summary of Formal Specification and Verification of Autonomous Robotic Systems. In *Integrated Formal Methods*, Wolfgang Ahrendt and Silvia Lizeth Tapia Tarifa (Eds.). Springer International Publishing, Cham, 538–541.
- [47] Alice Miller, Bernd Porr, Ivaylo Valkov, Douglas Fraser, and Daumantas Pagojus. 2025. Model checking with memoisation for fast overtaking planning. *Science of Computer Programming* 244 (2025), 103300. doi:10.1016/j.scico.2025.103300
- [48] Daumantas Pagojus, Alice Miller, Bernd Porr, and Ivaylo Valkov. 2021. Simulation and Model Checking for Close to Realtime Overtaking Planning. See [19], 20–37. doi:10.4204/EPTCS.348.2
- [49] Christian Pek, Stefanie Manzinger, Markus Koschi, and Matthias Althoff. 2020. Using online verification to prevent autonomous vehicles from causing accidents. *Nature Machine Intelligence* 2, 9 (01 Sep 2020), 518–528. doi:10.1038/s42256-020-0225-y
- [50] Gang Peng, Yicheng Zhou, Lu Hu, Li Xiao, Zhigang Sun, Zhangang Wu, and Xukang Zhu. 2023. VILO SLAM: Tightly Coupled Binocular Vision–Inertia SLAM Combined with LiDAR. *Sensors* 2023, Vol. 23, Page 4588 23, 10 (5 2023), 4588. doi:10.3390/S23104588
- [51] Bernd Porr and Florentin Wörgötter. 2005. Inside embodiment – what means embodiment to radical constructivists? *Kybernetes* 34, 1 (2005), 105–117. doi:10.1108/03684920510575762
- [52] P. J. Ramadge and W. M. Wonham. 1987. Supervisory Control of a Class of Discrete Event Processes. *SIAM Journal on Control and Optimization* 25, 1 (1987), 206–230. doi:10.1137/0325013 arXiv:https://doi.org/10.1137/0325013
- [53] Yingying Ran, Xiaobin Xu, Zhiying Tan, and Minzhou Luo. 2025. A Review of 2D Lidar SLAM Research. *Remote Sensing* 2025, Vol. 17, Page 1214 17, 7 (3 2025), 1214. doi:10.3390/RS17071214
- [54] Randall C. Smith and Peter Cheeseman. 1986. On the Representation and Estimation of Spatial Uncertainty. *The International Journal of Robotics Research* 5, 4 (1986), 56–68. doi:10.1177/027836498600500404 arXiv:https://doi.org/10.1177/027836498600500404
- [55] Elizabeth S. Spelke and Katherine D. Kinzler. 2007. Core knowledge. *Developmental Science* 10, 1 (1 2007), 89–96. doi:10.1111/J.1467-7687.2007.00569.X
- [56] Huihui Sun, Weijie Zhang, Runxiang Yu, and Yujie Zhang. 2021. Motion Planning for Mobile Robots—Focusing on Deep Reinforcement Learning: A Systematic Review. *IEEE Access* 9 (2021), 69061–69081. doi:10.1109/ACCESS.2021.3076530
- [57] Güliz Tuncay, Soteris Demetriou, Karan Ganju, and Carl A. Gunter. 2018. Resolving the Predicament of Android Custom Permissions. In *Network and Distributed System Security Symposium*. 1–15. doi:10.14722/ndss.2018.23221
- [58] Moshe Y. Vardi. 1988. An automata-theoretic approach to protocol verification. In *CONCURRENCY 88*, Frederich H. Vogt (Ed.). Springer Berlin Heidelberg, Berlin, Heidelberg, 73–73.
- [59] L. Wang and F. Cai. 2017. Reliability analysis for flight control systems using probabilistic model checking. *Proceedings of the IEEE International Conference on Software Engineering and Service Sciences, ICSESS 2017-Novem (2017)*, 161–164. doi:10.1109/RAM.2017.7889773
- [60] Weichen Wei, Bijan Shirinzadeh, Rohan Nowell, Mohammadali Ghafarian, Mohamed M.A. Ammar, and Tianyao Shen. 2021. Enhancing Solid State LiDAR Mapping with a 2D Spinning LiDAR in Urban Scenario SLAM on Ground Vehicles. *Sensors* 2021, Vol. 21, Page 1773 21, 5 (3 2021), 1773. doi:10.3390/S21051773
- [61] M. Weißmann, S. Bedenk, C. Buckl, and A. Knoll. 2011. Model Checking Industrial Robot Systems. In *Model checking software (SPIN 2011)*, Vol. 6823. Springer Berlin Heidelberg, 161–176.
- [62] Kelvin Wong, Yanlei Gu, and Shunsuke Kamijo. 2021. Mapping for Autonomous Driving: Opportunities and Challenges. *IEEE Intelligent Transportation Systems Magazine* 13, 1 (2021), 91–106. doi:10.1109/ITS.2020.3014152
- [63] Bin Zhang, Zexin Peng, Bi Zeng, and Junjie Lu. 2024. 2DLIW-SLAM: 2D LiDAR-inertial-wheel odometry with real-time loop closure. *Measurement Science and Technology* 35, 7 (4 2024), 075205. doi:10.1088/1361-6501/AD3EA3